Geological Field Trips and Maps

2026
Vol. 18 (1.2)

The granite-migmatite connection in Variscan northern Sardinia

https://doi.org/10.3301/GFT.2026.02

SOCIETÀ GEOLOGICA ITALIANA ETS
FONDATA NEL 1881 - ENTE MORALE R. D. 17 OTTOBRE 1885

ISPRA
Istituto Superiore per la Protezione e la Ricerca Ambientale

Sistema Nazionale per la Protezione dell'Ambiente

Geological Field Trips and Maps

Periodico semestrale del Servizio Geologico d'Italia - ISPRA e della Società Geologica Italiana ETS
Geol. F. Trips Maps, Vol. **18** No.1.2 (2026), 40 pp., 26 figs. (https://doi.org/10.3301/GFT.2026.02)

The granite-migmatite connection in Variscan northern Sardinia

Leonardo Casini[1], Silvio Ferrero[2], Francesco Secchi[1,3], Alfredo Idini[2], Gabriele Cruciani[2], Olga Turek[2] & Paola Mameli[1]

[1] Università di Sassari, Dipartimento di Scienze Chimiche, Fisiche, Matematiche e Naturali via Vienna 2 - 07100 Sassari (Italy).
[2] Università di Cagliari, Dipartimento di Scienze Chimiche e Geologiche S.S. 554 Cittadella Universitaria - 09042 Monserrato (Italy).
[3] IGAG - CNR - Sede Secondaria di Roma, c/o Dipartimento di Scienze della Terra, Sapienza Università di Roma, Roma (Italy).

LC, 0000-0002-6157-1865; SF, 0000-0002-9948-3676; FS, 0000-0002-0357-1808; AI, 0000-0002-9937-5149; GC, 0000-0002-6624-5655; OT, 0000-0001-5263-4556; PM, 0000-0003-3236-6472.

Corresponding e-mail address: casini@uniss.it

Cover page figure: The Stretti area (Asinara Island, Sassari Province), on the western coast of the island, as seen from the south. The cliff exposes highly strained mylonitic paragneiss and quartzite wrapping around amphibolite boudins that have been deformed within a major late-Variscan shear zone (Carboniferous-Permian).

ISSN: 2038-4947 [online]

http://gftm.socgeol.it/

INDEX

INFORMATION

EXCURSION NOTES

ITINERARY

ABSTRACT

Northern Sardinia exposes a remarkably continuous section of Palaeozoic continental crust minimally affected by post-Variscan tectonics. The Variscan crust includes lower crustal migmatites with relic of high-pressure – high-temperature granulitic assemblages (P=1.2–2.2 GPa, T>800°C), middle crustal metapelite, amphibolite, and calc-alkaline orthogneiss derived from reworking of a thick Ordovician magmatic arc. These metamorphic rocks are intruded by the late Palaeozoic (Carboniferous-Permian ~340-280 Ma) Corsica-Sardinia Batholith, a roughly 500 km-long, 50 km-wide composite magmatic province formed incrementally by emplacement of several plutons during post-orogenic extension and tectonic reorganisation of major lithospheric blocks related to shearing of Pangaea. In this 5-days field trip, we will explore the migmatite-granite transition zone and four plutons emplaced at different depths, focusing on the relative contribution of crustal reworking and mantle melting for the evolution of the continental crust. More technical topics about the emplacement mechanisms, length scales and timescales of magmatism, and the competition between different chemical and physical processes during the assembly of granitic plutons will also be discussed in relation to specific structures and rock compositions.

Keywords: granite petrology, pluton emplacement, HT metamorphism, shear zones, partial melting.

PROGRAM SUMMARY

The outcrops visited during the five-days field trip are localised in two distinct areas of Sardinia (Fig. 1a). The first area is in NW Sardinia (Asinara Island, days 1-2, Fig. 1b) and should be reached from Porto Torres by daily ferry boat (crossing is about 1h 45'). As the Asinara island is a national park and marine protected area, private motor vehicles are not allowed and the transfers between the various outcrops should be done by walking, bicycling, or using electric vehicles that could be rent on site. The outcrops visited during the first two days of the field trip are generally close to the road and require less than 5 min walking on well-marked footpath. Although there are options to stay overnight in the Asinara Island, this possibility must be checked because of the limited number of available places, particularly during the winter months. The second area object of this field trip is in NE Sardinia and touches several localities between S. Teresa di Gallura and Arzachena village (days 3-5, Fig. 1c). These areas should be reached by car from Porto Torres, following the SS134 road (Fig. 1a). The outcrops visited during the last three days of the field trip require some 5-15 minutes hiking from the car, generally on good footpaths with minimal overall height differences (<100 m) on distances less than 500-600 m.

Day 1 - The Variscan crustal roots of northern Asinara Island and the Posada-Asinara shear zone
Stop 1.1 - Migmatites, amphibolites and peraluminous granite - Punta Sabina
Stop 1.2 - Mylonitic orthogneiss with Silurian protolith age - Cala d'Oliva
Stop 1.3 - Andalusite-garnet-staurolite-bearing micaschists - Ossario
Stop 1.4 - Mylonitic paragneisses and amphibolites of the Posada-Asinara Line - Li Stretti
Day 2 - The Castellaccio megacrystic pluton
Stop 2.1 - Andalusite hornfels along the northern border zone - Punta Sa Nave
Stop 2.2 - K-feldspar cumulates and flow structures in the wall-roof transition zone - Tumbarino
Stop 2.3 - The chilled margin in the southern border zone - Fornelli
Stop 2.4 - Aplitic and granitic dykes - Punta Pedra Bianca
Day 3 - The migmatitic complex
Stop 3.1 - Garnet-bearing diatexite and amphibolite - Punta Bianca
Stop 3.2 - Amphibole-bearing granodiorite - Punta Bianca
Stop 3.3 - Co-seismic deformation structures related to water-fluxed melting - Punta Bianca
Stop 3.4 - Contact between S. Teresa monzogranite and the Barrabisa pluton - Punta Bianca

Day 4 - Late Variscan magmatism through the Carboniferous-Permian boundary
Stop 4.1 - The roof of Arzachena pluton - Mt Mazzolu quarry - Arzachena
Stop 4.2 - The wall-floor transition zone - S. Giacomo, SdF quarry - Arzachena
Stop 4.3 - The granodioritic core of the Arzachena pluton - Punta Candela
Stop 4.4 - The La Ettica Permian gabbro and quartz-diorite - Punta La Ettica
Stop 4.5 - Magmatic breccias along the southern border zone - S. Paolo Calta
Day 5 - post-Variscan extension and mafic magmatism - the Punta Falcone magmatic complex
Stop 5.1 - Border of the Punta Falcone mafic complex - Punta Falcone
Stop 5.2 - Gabbro-diorite dykes of the feeder zone - Punta Falcone

SAFETY

Most outcrops can be easily reached hiking with no danger or particular access difficulties, except stops 4.2 and 4.3 which are within the perimeter of active quarries and can be visited only upon permission from their respective owners. However, equivalent outcrops can be observed near the entrance of the quarries. Days 1 and 2 take place within the Asinara National Park where sampling is not allowed and there are also specific restrictions related to environmental protection. More information here: https://www.parcoasinara.org/en/.

The weather in northern Sardinia is usually dry and windy with temperatures rarely below 14°C, also during the winter. Hiking is possible all year round, however summer (July-August) is not recommended for excessive heat and sun.

HOSPITALS

Ospedale Giovanni Paolo II, Via Bazzoni - Sircana, 2/2A, 07026 Olbia SS, +39 0789 552200

Ospedale Civile Santissima Annunziata, Via Enrico de Nicola, 39, 07100 Sassari, +39 079 206 1000

ACCOMMODATION

For the overnight stay, northern Sardinia is a renowned turistic place and there are several options ranging from camping to five stars hotels. For the organisation of this guide it is suggested to sleep in the following villages: day 1-2 Porto Torres, day 3-5 S. Teresa di Gallura.

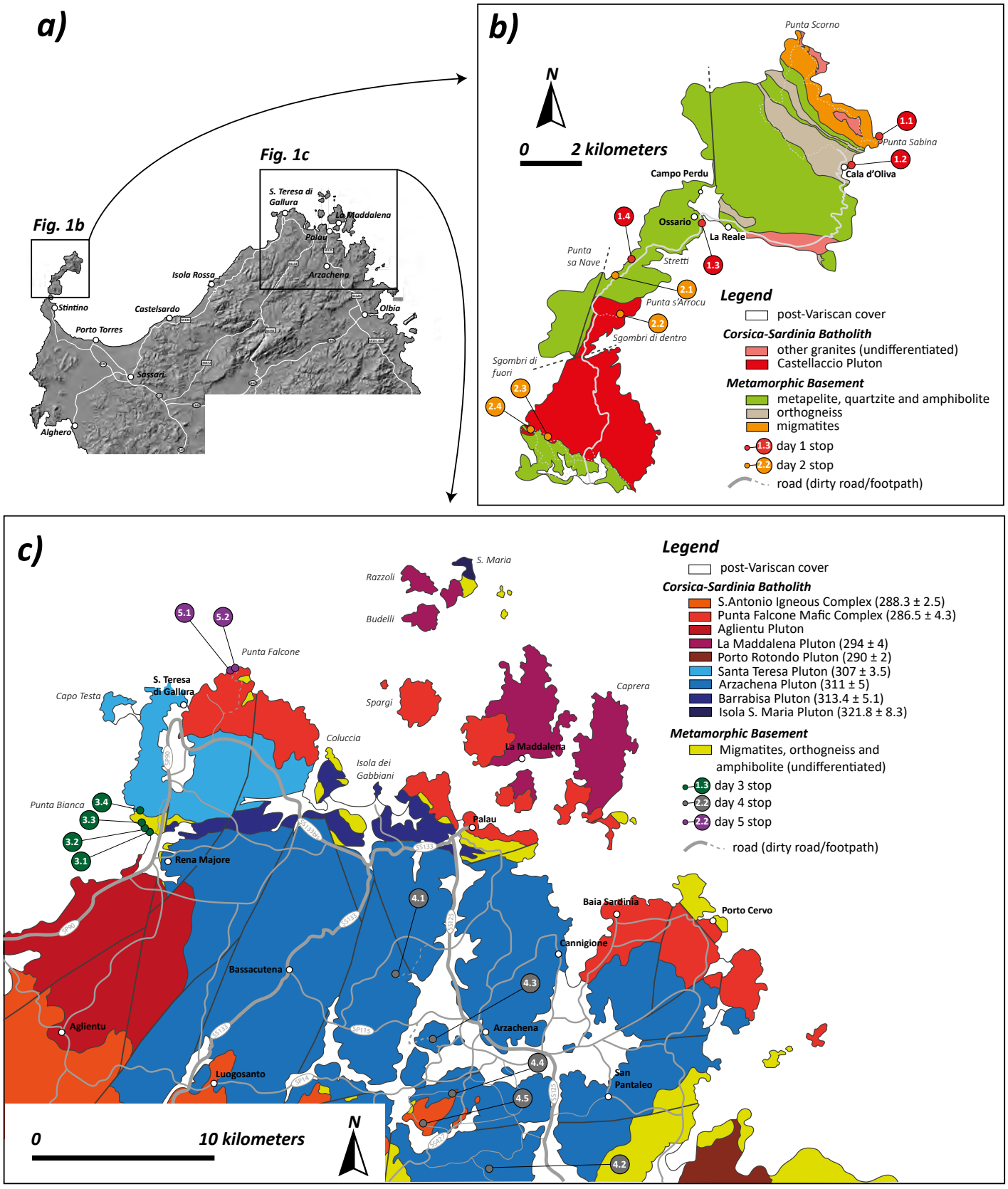

Fig. 1 - Organisation of the field trip: a) Digital Elevation Model of N Sardinia showing the principal cities and the location of the areas subject of the five-days field trip, b) simplified geological map of Asinara Island (modified from Cuccuru et al., 2018; Carosi et al., 2024) showing the location of the stops of the first two days of the field trip, c) simplified geological map of NE Sardinia showing the location of the outcrops visited during the last three days of the field trip, and the principal roads (grey lines) and footpaths (dashed grey lines).

INTRODUCTION

Sardinia exposes one of the most continuous and best-preserved Palaeozoic sections of southern Europe, thus offering a unique opportunity to observe the anatomy of an ancient orogenic system, the Variscan chain. The segment of the Variscan orogen that crops out in Sardinia consists of three distinct structural domains including the high-grade metamorphic roots exposed in the North, the low-grade metamorphic wedge in central Sardinia, and the non-metamorphic fold and thrust belt foreland that crops out in the south-western sector of the island (i.e., Carmignani et al., 1994). The Variscan section of Sardinia includes also a late-orogenic batholith, the Corsica-Sardinia Batholith (C-SB; Rossi & Cocherie, 1991), formed by several plutons and volcanic complexes emplaced episodically during the Carboniferous-Permian transition (340-280 Ma; Casini et al., 2012; 2015a; Padovano et al., 2014; Paquette et al., 2003). The C-SB, altogether with the Central Iberia Batholith, the Bohemian Batholith, and the crystalline massifs scattered along the south Alpine basement of the Alps is one of the largest (500 km-long, 60-80 km-wide) magmatic provinces preserved in Variscan Europe. Due to excellent exposure and nearly absent post-Variscan deformation, the C-SB offers a privileged perspective on the architecture of trans-crustal magmatic systems, from the migmatitic-granulitic source zone to mid-crustal plutons, and finally to plutonic-volcanic massifs at even shallower depth. The diversity of melt compositions, emplacement conditions, and relations between magmatic systems and regional tectonic and metamorphic events make the C-SB an ideal place to investigate different geologic topics, including the relative role of mantle and crust for the generation of granitic magmas, the lifetime of magmatic processes, the plutonic-volcanic connection, and the feedbacks between magmatism, geochemical evolution of the continental crust, and ore formation.

GEOLOGICAL SETTING

The Sardinian segment of the South Variscan belt (Fig. 2a) shows an almost complete orogenic section, from the high-grade migmatitic Inner Zone in the northeastern sector of the island to the very low-grade External Zone exposed in the southwest (Carmignani et al., 1994; Rossi et al., 2009). A thick pile of allochthonous greenschist to lower-amphibolite facies metamorphic units, collectively identified as the Nappe Zone, is exposed in the central part of the island. The migmatitic Inner Zone with relic granulitic and eclogitic assemblages is separated from the amphibolite to greenschist-facies tectonic units of the Nappe Zone and the External Zone by a major NW-SE strike-slip shear zone with top-to-the E sense of tectonic transport (Posada-Asinara Line, PAL, Fig. 2b;

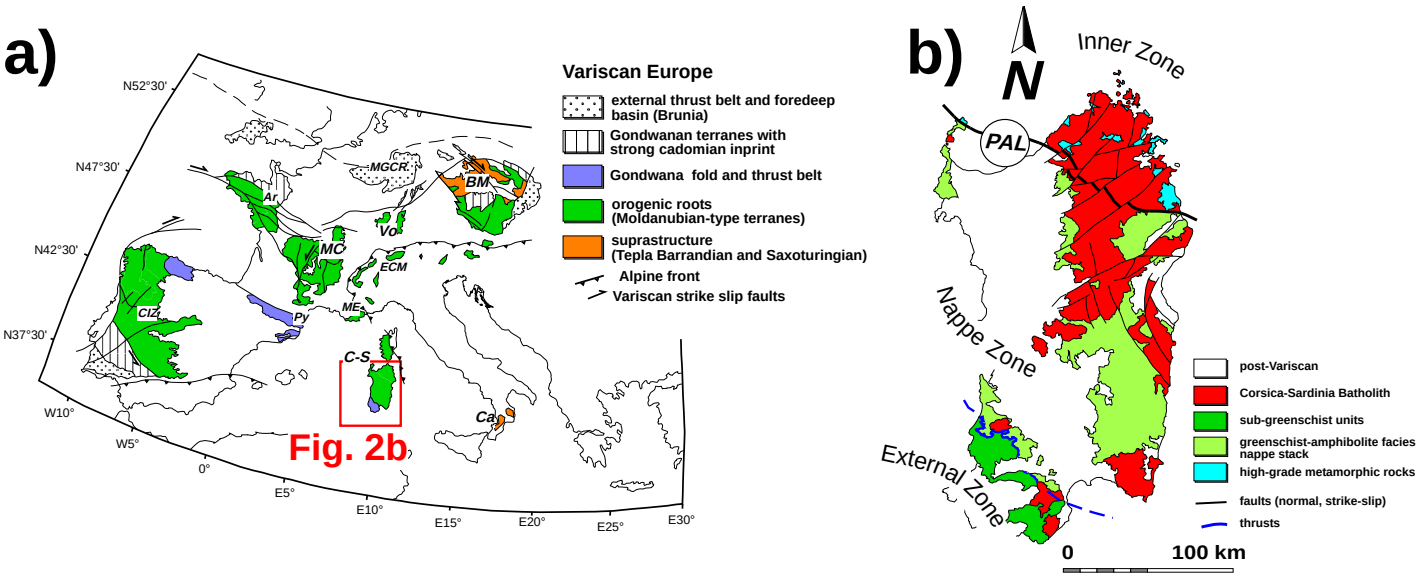

Fig. 2 - Geological setting: a) simplified geological map of Variscan massifs in Europe, modified from Martinez Catalan et al. (2021); CIZ – Central Iberian Zone, Py – Pyrenees, MC – French Massif Central, Ar – Armorican Massif, ME – Maures-Esterel Massif, C-S – Corsica-Sardinia Massif, ECM – External Crystalline Massifs of the Alps, Vo – Vosges Massif, Ca – Calabria, MGCR – Mid-German Crystalline Raise, BM – Bohemian Massif, b) simplified geological map of Variscan Sardinia, PAL – Posada-Asinara Line.

Elter et al. 1990; Carosi & Palmeri 2002). Ar-Ar dating of muscovite and U/Th-Pb dating of monazite in mylonitic paragneisses constrain the age of crustal shearing, locally under transpressional regime, between about 320 and 305 Ma (Di Vincenzo et al., 2004; Carosi et al., 2012), matching the age of syntectonic peraluminous cordierite + muscovite ± garnet-bearing plutons emplaced within E-W sinistral and NW-SE dextral shear zones of the Inner Zone (Casini et al., 2012, 2015a,b, 2023; De Luca et al., 2023). The occurrence of metabasite boudins with relic HP mineral assemblages of Devonian age (Cortesogno et al., 2004; Palmeri et al., 2004; Giacomini et al., 2005; Cruciani et al., 2024) has led some authors to interpret the PAL as a segment of the eo-Variscan suture zone active during the Devonian and up to the early Carboniferous (i.e., Cappelli et al., 1992; Carmignani et al., 1994). This interpretation is broadly consistent with the Silurian age of the metabasite protoliths and their geochemical N-MORB fingerprint (Cappelli et al., 1992). Yet, the relatively low pressure recorded by metabasite and the absence of rocks characterised by clear oceanic affinity led several authors to interpret the PAL as a backthrust (Helbing et al., 2006) or a transcrustal and transpressional orogen-parallel shear zone (Giacomini et al., 2006; Carosi et al., 2012; Graziani et al., 2020). Due to the incompleteness of geochronological, palaeomagnetic and structural datasets, different geodynamic models have been proposed to correlate the Corsica-Sardinia block and the Variscan terranes of continental Europe (Matte, 2001; Von Raumer et al., 2003; Rossi et al., 2009; Oggiano et al., 2010). The most comprehensive and up to date palaeogeographic reconstructions integrate the position and lifetime of the Ordovician arc, the age of Variscan HP metamorphism, the association of fossil faunae, and the age and magnetic fabric orientation of late-Variscan granites (Edel et al., 2014). Based on these models, the Inner Zone and the greenschist to amphibolite facies tectonic units of the Nappe Zone represent the orogenic infrastructure (Fig. 2a) corresponding to the Moldanubian domain widely exposed from the Bohemian massif to the French Massif Central and the Iberian massif. On the other side, the non-metamorphic sequences of the External Zone correspond to the suprastructure developed onto the northern Gondwana margin (Martinez-Catalan et al., 2021; Cocco et al., 2022). The Variscan crust of Sardinia is intruded by the Corsica-Sardinia Batholith (C-SB; Ghezzo & Orsini, 1982; Rossi & Cocherie, 1991), an 80-km wide magmatic province composed of several late-orogenic and post-orogenic plutons and volcanic complexes emplaced episodically between early Carboniferous and Permian times (340-280 Ma; Casini et al., 2012, 2015a; Padovano et al., 2014; Paquette et al., 2003).

PRE-VARISCAN HISTORY

The pre-Variscan history is best preserved in the southwestern part of the island, where Variscan deformation is only locally pervasive, and metamorphism does not exceed sub-greenschist facies conditions. The Cambrian to early Carboniferous stratigraphic sequences preserve a main pre-Variscan angular unconformity separating an early Palaeozoic sedimentary sequence from the thick early-Middle Ordovician magmatic arc and the Upper Ordovician meta-volcanic rocks and metasediments derived from its reworking (Oggiano et al., 2010; Gaggero et al., 2012). The middle Paleozoic successions (Silurian-Devonian) testify a major geodynamic change, outlined by the occurrence of shallow-marine sediments followed by carbonaceous black shales and marbles. The early Palaeozoic history is barely preserved in the Inner Zone, because of the HT metamorphism, extensive Variscan deformation and post-orogenic magmatism. However, xenocrystic zircons of migmatites and late-Variscan (Carboniferous-Permian) granites commonly preserve cores with inherited pre-Variscan ages (i.e., Giacomini et al., 2005, 2006; Casini et al., 2023; De Luca et al., 2023). Most of these xenocrysts preserve Early to Middle Ordovician ages (485-460 Ma) and show clear magmatic oscillatory zoning (i.e., Casini et al., 2015b, 2023). This observation and the common occurrence of calcalkaline magmatic protoliths in the migmatitic complex suggest reworking of the Ordovician magmatic arc, which is widely exposed in the Nappe Zone to the south of the Posada-Asinara Line (i.e., Oggiano et al., 2010; Pavanetto et al., 2012; Cruciani et al., 2013, 2018; Gaggero et al., 2017). Much older zircons ranging in age from Silurian to Meso-Archean are also occasionally reported within migmatites and amphibolite-facies metasediments (i.e., Cruciani et al., 2020). A systematic study about the frequency and spatial distribution of inherited pre-Variscan, and particularly pre-Ordovician, ages is still lacking, though, and this makes it difficult to correlate the early Palaeozoic successions of the Inner Zone with the Nappe Zone.

VARISCAN TECTONIC AND METAMORPHIC EVENTS

The Variscan architecture results from a long-lasting sequence of tectonic and metamorphic events related to Devonian–early Carboniferous subduction of a Palaeozoic oceanic domain (i.e., crypto-Rheic ocean, Von Raumer et al., 2003; South Armorican Ocean, Ballevre et al., 2009), followed by a Carboniferous oblique collision between a narrow ribbon-like continental domain and the northern

margin of Gondwana (Carmignani et al., 1994; Von Raumer et al., 2003; Rossi et al., 2009; Oggiano et al., 2010). Finally, during late Carboniferous (320–300 Ma; Edel et al., 2014), the whole orogen experienced a major phase of tectonic reorganisation accommodated by lithospheric-scale shear zones (Carosi & Palmeri 2002; Gumiaux et al., 2004; Siebel et al., 2004; Denèle et al., 2008; Casini & Funedda, 2014) developed in response to self-subduction of the incipient global Pangaea plate (Gutierrez-Alonso et al., 2008). The sequence of deformation phases is well preserved in the low-grade metamorphic nappe stack exposed in the central and south-eastern part of Sardinia, though it is still poorly correlated with the evolution of the high-grade crystalline crust exposed to the north of the Posada-Asinara Line (Fig. 3). The main shortening phase is characterised by top-to-the S or SSW direction of tectonic transport (D_1 – Carmignani et al., 1994; Gerrei and Meana Phases – Conti et al., 2001) and resulted in the stacking of tectonic units and a prograde metamorphism. The main structures related to the D_1 phase are south-verging isoclinal folds and thrusts, well preserved in the Nappe Zone and in the External Zone. Metamorphism associated with D_1 and D_2 deformation is marked by the appearance, at progressively deeper structural levels, of biotite, garnet + oligoclase, staurolite + kyanite/sillimanite assemblages in metapelitic rocks (Franceschelli et al., 2005 and references therein). In the axial zone, due to extensive anatexis and superposition of late-orogenic deformations, D_1 structures are generally not recognizable in the field, although occasionally preserved within large orthogneisses or mafic/ultra-mafic bodies. The age of D_1 is not precisely constrained

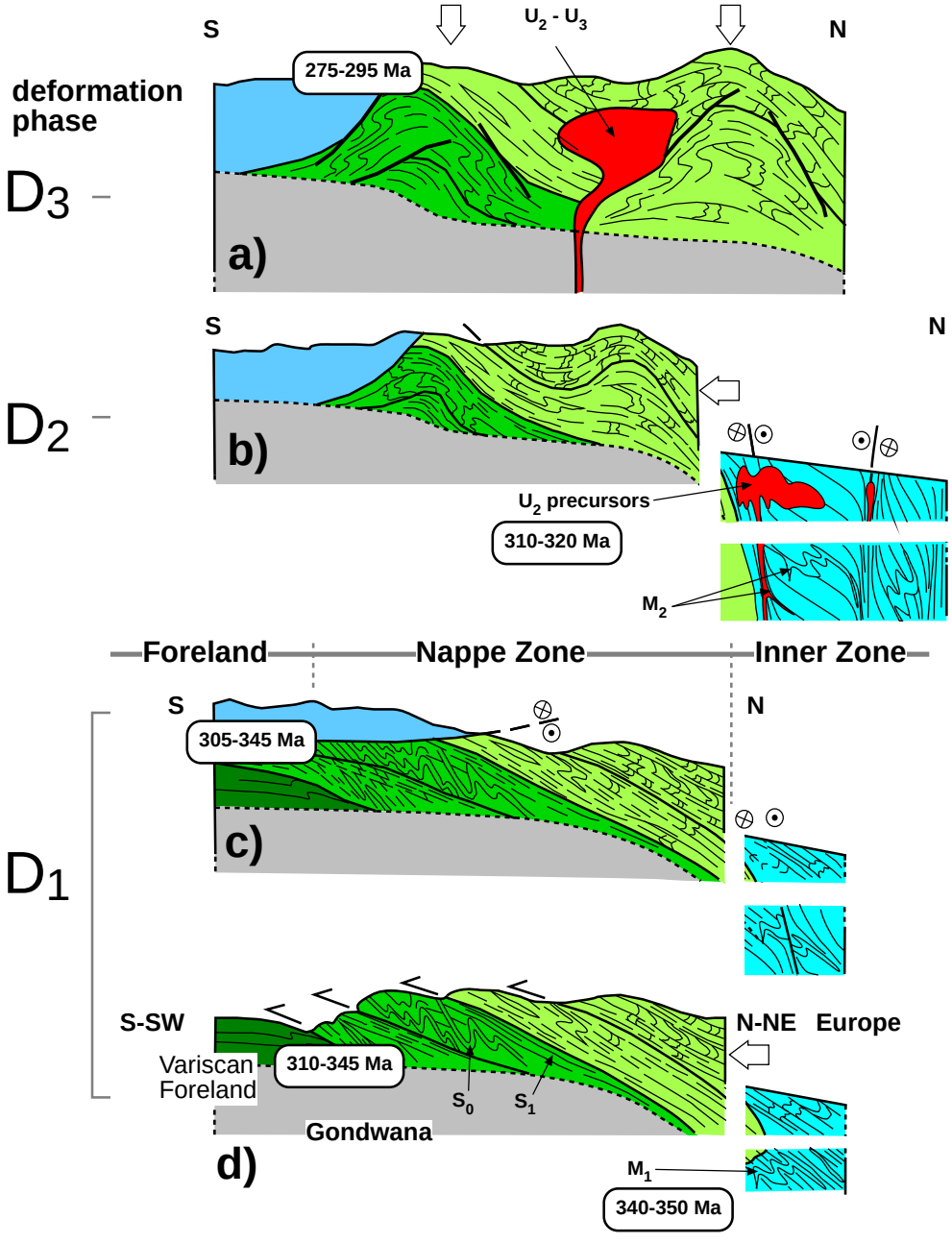

Fig. 3 - Sequence of Variscan deformation phases and structure development showing the tentative correlation between Nappe Zone and high-grade Inner Zone; S_0 – bedding, S_1 – metamorphic foliation. Dark green – Variscan Foreland, green – External Nappes, light green – Internal Nappes, cyan – migmatitic Inner Zone, red – late-Variscan granites, blue - out-of-sequence Sarrabus Unit. The white arrows indicate the inferred direction of regional ?1, the thin black arrows indicate the direction of tectonic transport of the main thrusts.

in the greenschist Nappe Zone, however Ar/Ar dating of amphibole and muscovite from sheared metabasites and micaschists of northern Sardinia suggest that deformation occurred between about 360–340 Ma (Ferrara et al., 1978; Di Vincenzo et al., 2004). This age fits the onset of the first melting stage M_1 in N Sardinia, which has been constrained between about 355 and 345 Ma (Ferrara et al., 1978; Giacomini et al., 2006, 2008; Casini et al., 2023; Cruciani et al., 2024).

A second shortening phase is characterised by top-to-the W-SW direction of tectonic transport (D_2 - Carmignani et al., 1994; Sarrabus Phase – Conti et al., 2001). In the Nappe Zone, D_2 gives way to orogen-perpendicular thrusting of the Sarrabus Unit under retrograde lower greenschist facies conditions (Conti et al., 2001). D_2 deformation in the Inner Zone is marked by extensive shearing under amphibolite facies conditions, testified by strongly asymmetric folds with N-S to NW-SE horizontal axis and mylonitic shear zones (Carmignani et al., 1994; Carosi & Oggiano, 2002; Carosi et al., 2004). The last shortening phase D_3 (Flumendosa Phase – Conti et al., 2001) produced, in the Nappe Zone, km-scale open synforms and antiforms oriented from NW-SE to roughly W-E in the very southern part of the Nappe Zone. These structures, still undated, developed under diagenetic or very low-grade metamorphic conditions and are not associated with penetrative foliations. The D_3 phase has been tentatively correlated with the development, under greenschist facies retrograde conditions, of upright folds and kink bands in the Inner Zone (Carosi & Oggiano, 2002; Carosi et al., 2004; Franceschelli et al., 2005).

Finally, the orogenic crust experienced gravitational re-equilibration leading to post-orogenic extension (D_4 - Rio Gruppa Phase – Conti et al., 2001), vertical shortening, and high-temperature – low-pressure (HT-LP) metamorphism (Conti et al., 1999; Casini & Oggiano, 2008). Several authors propose that extension triggered decompression melting of the upper mantle and lower crust, providing the magmatic source of the Corsica-Sardinia Batholith (Carmignani et al., 1994; Conti et al., 2001; Ferré & Leake, 2001; Carosi et al., 2004). Although this model fits the long-term geodynamic evolution of the orogen, the geochemical fingerprints of many plutons, structural analysis, and high-resolution geochronologic constraints challenge this interpretation as explained in the next section.

LATE-VARISCAN MAGMATISM AND ASSEMBLY OF THE CORSICA-SARDINIA BATHOLITH

The metamorphic basement is intruded by several plutons and sub-volcanic complexes collectively known as the C-SB (~340–280 Ma; Paquette et al., 2003; Casini et al., 2012; Casini et al., 2015a,b; Cuccuru et al., 2016). Field structural analysis and U-Pb zircon dating indicate that magmatic activity was mainly episodic, clustering into three partly overlapping timespans that correspond to distinct magmatic stages labelled U_1, U_2 and U_3 (Fig. 4; Casini et al., 2015a). The oldest magmatic rocks emplaced during the U_1 stage in the early Carboniferous (340–335 Ma) giving rise to a N-S oriented granitic massif exposed only in NW Corsica.

These rocks, also known as 'Durbachites' or 'Mg-K granites' have quite a distinctive mineralogical composition. The mafic terms are characterised by the assemblage K-feldspar + plagioclase + biotite + diopside + hornblende + quartz. Titanite and magmatic epidote are the most common accessory phases altogether with zircon. On the other side, the more felsic U_1 rocks contain K-feldspar + quartz + plagioclase + biotite ± hornblende ± epidote. The geochemical and isotopic composition of U_1 rocks is characterised by systematically high contents of transition metals (Sc, Ni, Co, Cr), high concentration of Large Ion Lithophile Elements (LILE: Rb, Sr, Ba, Cs), and high content of REE with moderately to highly fractionated patterns (Fig. 5). Zirconium is generally abundant between about 100 and about 1000 ppm and is negatively correlated with the SiO_2 content, whereas Mg# calculated as the ratio $MgO/(Fe_2O_{3tot}+MgO)$ is always above 0.22 also in the more felsic rocks (Fig. 5e). Moreover, the U_1 rocks generally display relatively high, crustal-like, $^{87}Sr/^{86}Sr$ ratio around 0.707-0.708 and slightly negative to positive εNd values (Fig. 5f) between -3 and +1 (Cocherie et al., 1994). These mantle- and crust-derived hybrid features likely reflect mixing and assimilation of hydrous melts derived from a fertilised sub-continental mantle and lower crustal material (Rossi & Cocherie, 1991; Ferré & Leake, 2001). U_1 plutons show a broad range of fabric development, which is apparently correlated with the emplacement depth of the magmatic bodies, being more pervasive in the deeper intrusions. U_1 intrusions injected within mid-crustal (0.4-0.6 GPa; Rossi & Cocherie, 1991; Ferrè & Leake, 2001), N-S, strike-slip shear zones, in fact, record extensive HT-solid state deformation marked by incipient quartz ribbons, K-feldspar and plagioclase sigma-shaped mantled porphyroclasts (Rossi & Cocherie 1991). On the other hand, U_1 sub-volcanic complexes are characterised only by weak magmatic shape-preferred orientation of mafic enclaves, biotite and K-feldspar phenocrysts (Laporte et al., 1986). Based on the structural setting, geochemical fingerprint, and emplacement age in relation to late-Variscan tectonics, U_1 granites have been interpreted as the hallmark of slab break-off at the end of Variscan collision (Von Raumer et al., 2014).

The second magmatic stage (U_2) is widespread in the Corsica-Sardinia massif, producing a variety of calc-alkaline plutons

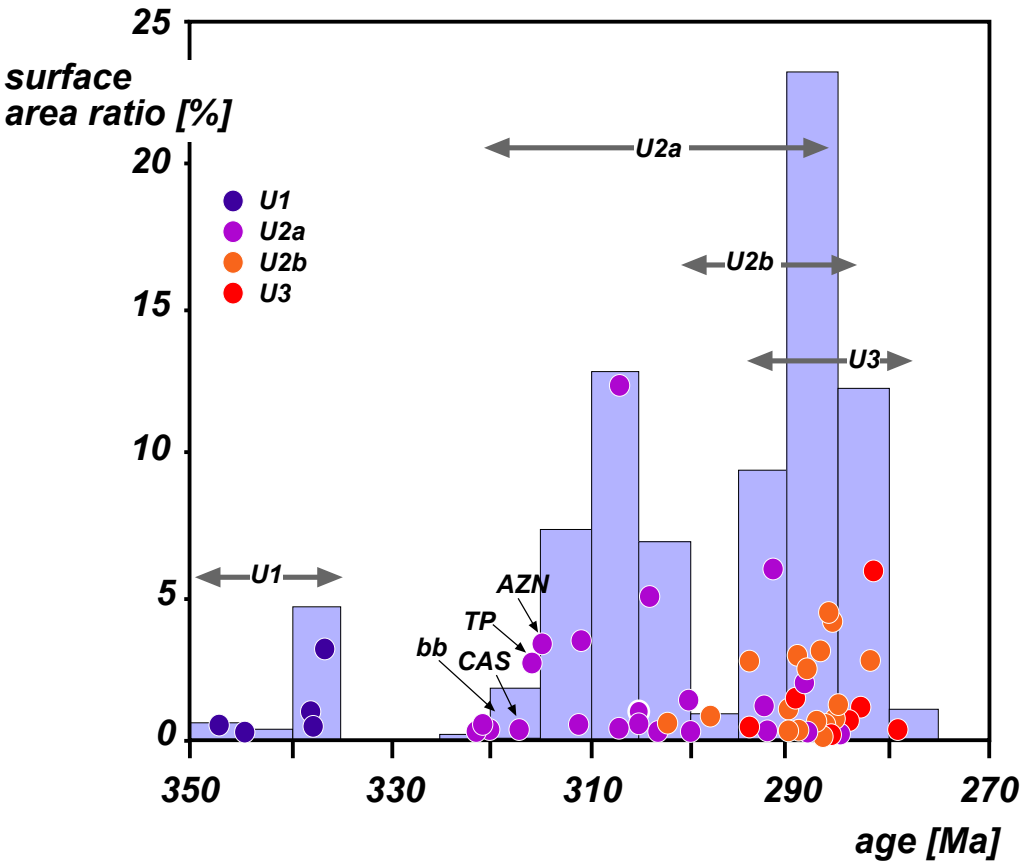

Fig. 4 - Age/surface area ratio plot showing the distribution of U_1-U_3 plutons during the time span 350-270 Ma. The surface area ratio value indicates the proportion between cumulative surface area of plutons accumulated during a given time span relative to the total surface area of the batholith. Bin size is 5 Myrs.

and sub-volcanic complexes. The emplacement age of most of these plutons ranges between middle Carboniferous–early Permian (~325-275 Ma; del Moro et al., 1975; Rossi & Cocherie, 1991; Paquette et al., 2003; Oggiano et al., 2005; Casini et al, 2012, 2015a). The U_2 magmatic stage reflects two partially overlapping sub-stages defined on the basis of structural and geochronological constraints. The first (U_{2a}, 325–300 Ma, Oggiano et al., 2005; Casini et al., 2012, 2015a,b, 2023) results into moderately to strongly peraluminous felsic to intermediate plutons (Fig. 5b) injected within NW-SE and E-W shear zones (Oggiano & Di Pisa, 1988; Casini et al., 2012, 2015a,b, 2023; Secchi et al., 2022; De Luca et al., 2023). The mantle component is apparently very low in these U_2 precursors (Fig. 5), as indicated by the low MgO and Zr contents, low Mg# below 0.2, nearly absent Ni, Co, Cr and Sc, highly negative εNd values also in the relatively mafic terms (εNd < -4; Fig. 5f), and absence of micro-granular mafic enclaves (Casini et al., 2015a). The U_{2a} granites form either small, ribbon-shaped, highly strained intrusions characterised by a pervasive magmatic to solid-state steep foliation parallel to the margin of the shear zone they inject into (i.e., Casini et al., 2023; De Luca et al., 2023), or large (>40 km-long, 3-8 km-thick) elliptical sills emplaced at middle to upper structural levels (0.2-0.4 GPa; Casini et al., 2012, 2015a,b, 2025).

The second sub-stage U_{2b} is bracketed between 305–280 Ma based on recent LA-ICP-MS U-Pb zircon dating (Gaggero et al., 2017; Casini et al., 2012, 2015a,b). The late-U_2 magmatism includes both highly differentiated felsic rocks and mafic terms. These latter form small batches and diapirs of gabbro, quartz-diorites to granodiorites and tonalites, often difficult to recognize in the field due to selective weathering. The mafic rocks are generally sub-alkaline to alkaline (Fig. 5a) and contain amphibole, clinopyroxene, locally partly corroded olivine. The major and trace-elements composition of gabbroic rocks indicates an origin from an enriched sub-continental mantle (Poli & Tommasini, 1991). The felsic component forms sub-volcanic complexes and upper-crustal plutons, which are emplaced at very low pressure, generally <0.2 GPa. The geochemical composition of U_{2b} felsic rocks is extremely heterogeneous ranging from K-rich strongly peraluminous muscovite + garnet-bearing syenogranites to metaluminous granodiorite. The εNd recalculated at the age of emplacement is variable from moderately negative values (-2 to -3 εNd) to strongly negative values around -7 to -8 εNd (i.e., Casini et al., 2015a). Overall, the isotopic signature and the common occurrence of partly assimilated crustal xenoliths indicate that U_{2b} felsic rocks formed by mixing between primitive mantle-derived melts and a heterogeneous crustal source composed of metasediments and partly assimilated U_{2a} granites (Fig. 5). The structure of U_{2b} granitoids is quite variable, however the magmatic fabric is generally only weakly developed and sub-solidus

deformation features can be observed at places close to the contacts with the metamorphic basement or the older intrusions.

Finally, a third magmatic phase (U_3) marks the end of the late-Variscan magmatism leading to the emplacement of volcanic to sub-volcanic alkaline to sub-alkaline (Fig. 5a) complexes documented only in central-western Corsica (Rossi & Cocherie, 1991; Paquette et al., 2003; Bonin, 2007) and in part of northern Sardinia (i.e., Casini et al., 2015b). These U_3 complexes are compositionally variable ranging from strongly peraluminous to metaluminous (Fig. 5b), with Zr content from >2000 ppm down to about 50 ppm. The ∑REE is generally below 200 ppm with moderately to weakly fractionated patterns (Fig. 5d).

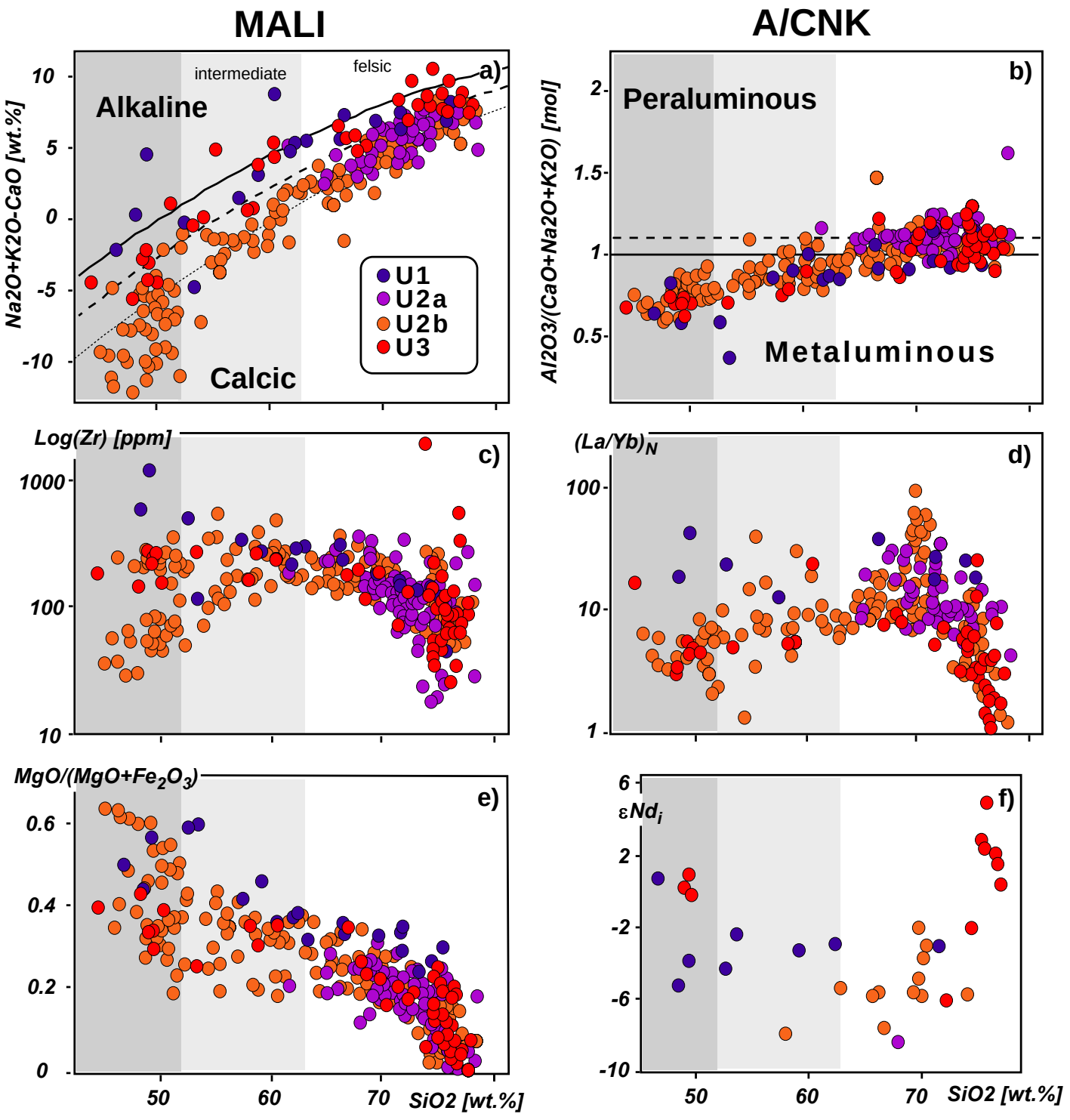

Fig. 5 - Summary of the geochemical characteristics of the C-S Batholith: a) MALI – Modified Alkali Lime diagram (Frost & Frost, 2008); b) A/CNK diagram (Sylvester, 1998); c)-f) Harker variation diagrams.

https://doi.org/10.3301/GFT.2026.02

DAY 1

THE VARISCAN CRUSTAL ROOTS OF NORTHERN ASINARA ISLAND AND THE POSADA-ASINARA SHEAR ZONE

The Asinara Island exposes the contact between the Nappe Zone and the migmatitic Inner Zone (Carosi & Oggiano, 2002; Carosi et al., 2004). The transition from low- to high-grade metamorphic units is marked by the switch from Barrowian oligoclase + garnet assemblages in the southern side of the Castellaccio Pluton to garnet + staurolite ± kyanite and finally K-feldspar + sillimanite assemblages going toward the north (Di Pisa et al., 1993; Carosi et al., 2004). The metamorphic rocks record a complex sequence of deformation structures that have been tentatively correlated with the regional deformation phases D_1-D_4. The oldest fabric (S_1), probably developed during continental collision, is preserved only as inclusion trails within garnet and oligoclase porphyroblasts (Carmignani et al., 1994; Carosi & Oggiano, 2002; Carosi et al., 2004; 2024). The dominant foliation observed in the field (S_2) is generally oriented E-W or NW-SE and may be locally mylonitic. This fabric has been related to post-collisional top-to-the east transpression (Carosi et al., 2004). Microstructural evidence suggests that the Barrowian metamorphic assemblages are from pre- to syntectonic with respect to the S_2 foliation (Franceschelli et al., 1982; Carosi & Palmeri 2002). The S_2 foliation is folded by E-W oriented F_3 upright open folds with an axial plane crenulation cleavage, which become progressively more pervasive in the northern part of the Island. Finally, localised F_4 kink folds with mainly sub-horizontal axial planes and brittle factures represent the latest brittle-ductile Variscan deformation structures (i.e., Carosi et al., 2004). To the north of the Castellaccio Pluton, HT-LP biotite ± andalusite/sillimanite assemblages partly replace the older Barrovian assemblages. This high-temperature metamorphic event has been related to decompression of the Variscan crust and upwelling of deep crustal magmas during the assembly of Corsica-Sardinia Batholith (i.e., Casini et al., 2025).

Stop 1.1 - Migmatites, amphibolite and peraluminous granite

Coordinates: Lat. 41°05'23"N, Long. 8°20'57"E
Location: Punta Sabina (Asinara, SS)

Punta Sabina can be reached following the footpath that start from the northern side of the Cala d'Oliva village close to the 'Hostel' (Fig. 1b). Punta Sabina and Cala dei Ponzesi, together with the remote Punta Scorno in the northern quadrant of Asinara Island, expose the deepest part of the Variscan crustal section. The Punta Sabina outcrop is a rocky cliff by the sea consisting of garnet + muscovite-bearing medium-grained peraluminous granite, quartz-rich aplitic dykes, and compositionally heterogeneous diatexite and metatexite. The main foliation of migmatites (S_2, Fig. 6a) is steep, oriented about NW-SE, and runs mostly parallel to the magmatic layering of peraluminous granites, which are interpreted as the anatectic product of partial melting during the D2 transpressional deformation phase (i.e., Carosi et al., 2004, 2006, 2024; Pieruccioni et al., 2025). Diatexites are plagioclase + biotite + garnet ± K-feldspar migmatite with variable melt to protolith ratio ranging from about 0.2 up to 0.9 and contain fragments of metatexite derived from a variety of protoliths. The most common metatexite type is plagioclase + K-feldspar + biotite ± sillimanite orthogneiss derived from Cambrian to Ordovician calc-alkaline granitoids (Fig. 6b; i.e., Casini et al., 2015b, 2023). Strongly foliated biotite + fibrolitic sillimanite ± garnet micaschists likely derived from partial melting of metapelites are also relatively frequent, though generally smaller than fragments derived from the orthogneiss (i.e., Cruciani et al., 2008). Finally, nearly pure quartzite and fine-grained amphibolite boudins can be observed within diatexites. These latter preserve evidence of an earlier migmatitic fabric pre-dating the magmatic flow layering of diatexite and contain the assemblage hornblende + grunerite + plagioclase ± titanite ± garnet (Fig. 6c). Biotite and quartz can also be observed at places, mostly within high-strain zones at the contact with metapelite or diatexites. In a small beach about 150 m to the southeast of Pta Sabina, diatexites grade into a small NW-SE oriented sill of peraluminous granite. The contact between the migmatitic complex and the granite is overall gradational and ductile, making it difficult to pinpoint the transition from metamorphic host rocks to the purely magmatic domain (Fig. 6a). The granite shows a nearly E-W to WNW-ESE weak magmatic flow foliation marked by the shape preferred orientation of biotite schlieren and rare K-feldspar phenocrysts. The assemblage of the granite is quartz + An_{25-40} plagioclase + K-feldspar + biotite ± muscovite. Apatite, zircon and ilmenite are common accessory phases. Quartz, plagioclase and K-feldspar show widespread evidence of HT crystal-plastic deformation such as chessboard pattern, stress twins, sub-grains, and lobate grain-boundaries (Figs. 7a,b).

https://doi.org/10.3301/GFT.2026.02

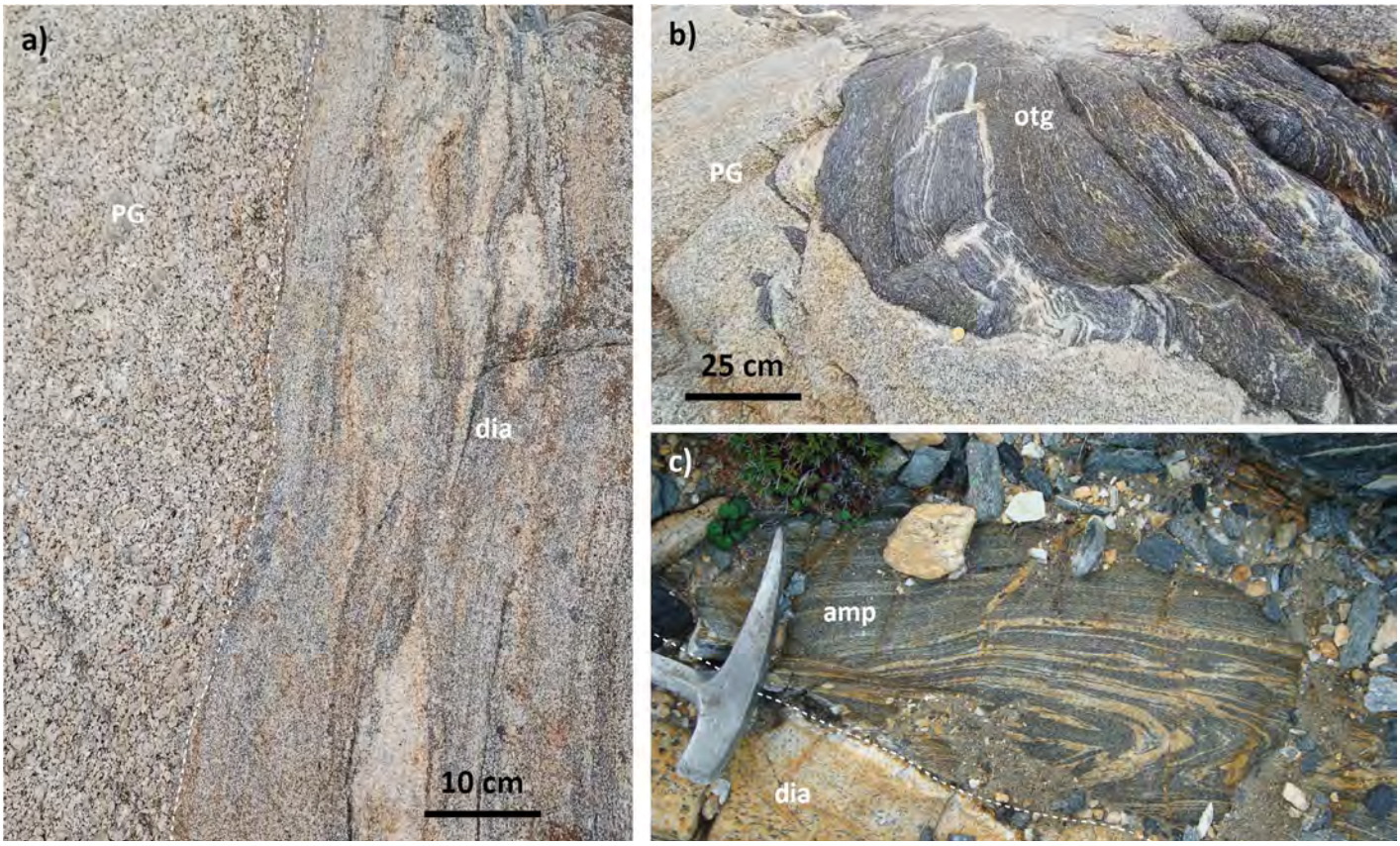

Fig. 6 - Migmatites and peraluminous granite of Punta Sabina: a) contact between medium-grained garnet + muscovite-bearing peraluminous granite (PG) and fine-grained heterogeneous diatexite (dia) showing an M_2 migmatitic foliation nearly parallel to the contact with the granite (white dashed line); b) migmatitic orthogneiss (otg) set within peraluminous granite (PG); note the migmatitic M_1 fabric of the orthogneiss is discordant relative to the contact with the granite; c) close-up of the migmatitic banding of amphibolite (amp) set within diatexite (dia).

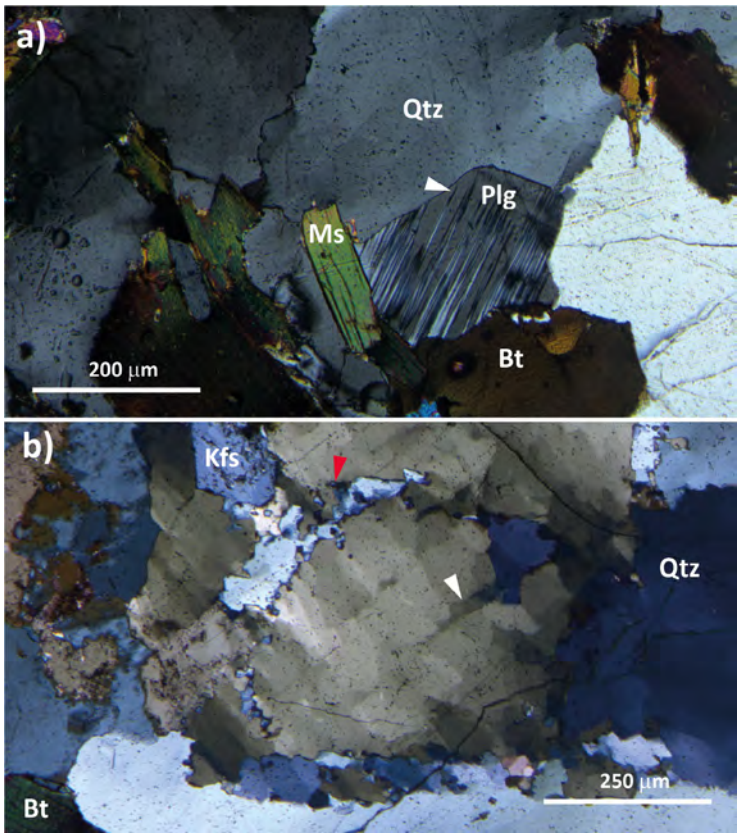

Fig. 7 - Microstructure of peraluminous granite: a) dominant assemblage of peraluminous granite including quartz (Qtz), biotite (Bt) and muscovite (Ms) flakes; plagioclase (Plg) commonly shows stress twins (white arrow); b) detail of a quartz-rich domain with the typical 'chessboard' structure (white arrow) and local development of subgrains along the quartz-quartz contacts (red arrow).

https://doi.org/10.3301/GFT.2026.02

Stop 1.2 - Mylonitic orthogneiss with Silurian protolith age

Coordinates: Lat. 41°04'49"N, Long. 8°20'21"E
Location: Lupertzio beach (Asinara, SS)

The Cala d'Oliva orthogneiss is exposed in a rocky wavecut platform to the west of the village and can be easily accessed following the footpath by the sea that goes northward from the small pier (Fig. 1b). The rock is a moderately to locally strongly foliated plagioclase + biotite + quartz + K-feldspar gneiss (Carosi et al., 2004, 2006) derived from metamorphism of a Silurian granodiorite that represents the youngest pre-Variscan magmatic protolith discovered so far in the Corsica-Sardinia massif (Rossi et al., 2009). The orthogneiss dominant fabric is the regional S_2 foliation (Fig. 8), which trends WNW-ESE in this outcrop, related to top-to-the SSW thrusting and dextral transpression during the D2 phase (i.e., Carosi et al., 2004; 2006; Di Vincenzo et al., 2004; Rossi et al., 2009). At places, an incipient S-C fabric can be observed. The orthogneiss is injected by several pegmatites characterised by quartz + K-feldspar + biotite ± tourmaline ± beryl assemblage, which clearly post-date the S2 fabric.

Stop 1.3 - Andalusite-garnet-staurolite-bearing micaschists

Coordinates: Lat. 41°03'46"N, Long. 8°16'49"E
Location: Ossario Austroungarico (Asinara, SS)

A few hundreds of m to the south of the war memorial, on a rocky beach easily accessible (10 m apart) from the road (Fig. 1b), a small cliff exposes garnet and staurolite-bearing micaschists (Carosi et al., 2004, 2006) that represent the pelitic Al_2O_3-rich term of the thick and monotonous sequence of metasedimentary rocks exposed in the middle segment of the Variscan crustal section, from Cala d'Oliva to the southern coast of Asinara. Micaschists are strongly deformed showing a pervasive S_2 foliation gently dipping toward ENE due to folding during the D3 phase of shortening (i.e., Carosi et al., 2004, 2006). Small intrafolial or rootless asymmetric F_2 folds marked by thin quartz-rich layers can be spotted throughout all the outcrop. The metamorphic assemblage consists of, in order of decreasing abundance, biotite + muscovite + quartz + garnet + andalusite + plagioclase ± staurolite ± tourmaline ± apatite ± zircon ± monazite ± graphite. Garnet is nearly pure almandine (X_{Alm} = 0.91-0.94) and contains inclusions of quartz, apatite, biotite, and albite-rich plagioclase (X_{ab} = 0.84–0.88). Biotite has an average 0.221 a.p.f.u. (atom per formula unit) of titanium recalculated on a 22 oxygens-formula, and the ratio of magnesium to the sum of magnesium and iron, X_{Mg}, ranges between 0.35 and 0.4. Prismatic andalusite crystals 1-5 cm-long are locally abundant and do not show any clear shape preferred orientation (Fig. 9a). Andalusite forms large post-tectonic porphyroblasts that overgrow S_2, commonly enclosing garnet, quartz, biotite and staurolite as inclusions (Fig. 9b). This microstructure indicates the HT-LP dehydration reaction: staurolite + muscovite + quartz = andalusite + biotite + H_2O. Micaschists are lepidoblastic rocks showing a strong NW-SE striking, NE-dipping, S_2 planar fabric marked by the preferred orientation of biotite and muscovite, and by a weak compositional layering defined by thin quartz +

Fig. 8 - Field structure and deformation fabric of the Cala d'Oliva orthogneiss.

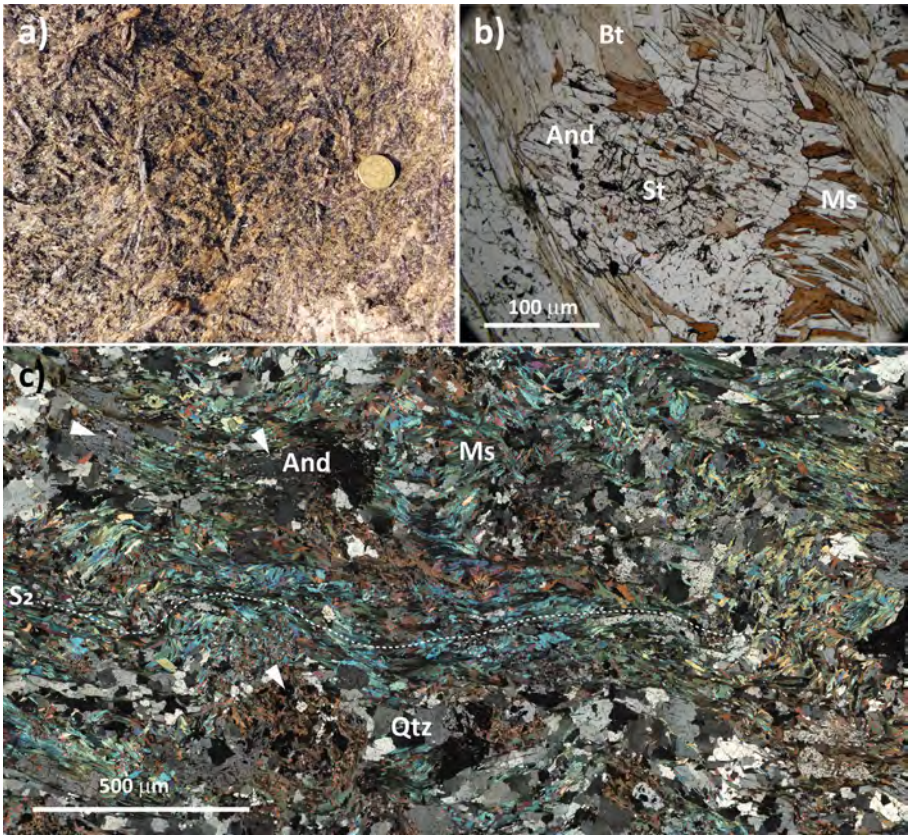

Fig. 9 - Andalusite-bearing micaschists: a) field aspect of micaschists showing the nearly random orientation of elongated andalusite porphyroblasts; b) inclusions of biotite (Bt), staurolite (St) within a large andalusite porphyroblast (And) partly surrounded by a rim of muscovite (Ms) and biotite, crossed polarizers; c) compositional layering of andalusite-bearing micaschists marked by quartz-rich bands alternating to mica-rich domains, the white arrows indicate some large andalusite porphyroblasts wrapped by the regional S_2 foliation (white dotted line).

plagioclase layers alternating with mica-rich domains. In some places, however, the S_2 foliation wraps andalusite porphyroblasts suggesting that HT-LP metamorphism is late-syntectonic relative to the dominant S_2 fabric (Fig. 9c).

Stop 1.4 - Mylonitic paragneisses and amphibolite of the Posada-Asinara Line

Coordinates: 41°03'03"N 8°15'05"E
Location: Stretti (Asinara, SS)

In the central portion of the Asinara Island, the middle-crustal metasedimentary sequence is intensely deformed within a steep E-W shear zone with top-to-the east direction of tectonic transport, related to localisation of deformation during D2 transpression. The shear zone anatomy is spectacularly exposed in a rocky cliff by the sea, that as an extra-bonus shows also a few boudins of weakly deformed amphibolites (Fig. 10). The outcrop can be reached from the road by walking toward the western coast of the island on easy terrain for a few tens of meters (Fig. 1b). The shear zone foliation is nearly parallel to the main S_2 foliation described in the northern part of the Island (see stops 1.1-1.3, Fig. 1b), however rootless hinges of isoclinal F_2 folds are still visible within the relatively low-strain domains of the shear zone, thus testifying the relative timing of structure development. The rocks are generally L- to L-S mylonites (Lister & Snoke 1984) derived from amphibolite-facies paragneisses and nearly pure quartzites alternating with thin, discontinuous, layers of andalusite-bearing micaschists. Massive amphibolite boudinsranging in size from a few cm to tens of m are widespread within the mylonitic belt and are remarkably well exposed along the cliffs of the western coast (Fig. 10). The major and trace element composition of amphibolite is consistent with derivation from N-MORB basalts (i.e., Cappelli et al., 1992), and their metamorphic mineral assemblage is composed of hornblende + plagioclase ± biotite ± garnet ± quartz ± titanite ± oxides. Amphibolites preserve evidence of an earlier, pre-shearing, HT fabric marked by plagioclase-rich bands and amphibole + oxides-rich domains, often at high angle with respect to the mylonitic fabric of the shear zone. High-temperature (T>650°C) conditions are consistent with microstructural evidence of grain-boundary diffusion in plagioclase and amphibole aggregates, and the chessboard pattern observed in quartz. Despite the lack of precise geochronologic constraints, this fabric could be tentatively correlated with the S_1/S_2 fabric preserved in metatexites (see Stop 1.1), as deformation within the shear zone is apparently related to decreasing temperature down to the stability field of chlorite + albite in the mafic bodies.

https://doi.org/10.3301/GFT.2026.02

Fig. 10 - Mylonitic paragneiss and quartzite within the Posada-Asinara shear zone, Li Stretti. Note the amphibolite boudins (white arrows) wrapped by the mylonitic foliation.

DAY 2

THE CASTELLACCIO MEGACRYSTIC PLUTON

The Castellaccio Pluton is a large (5×3 km), NW-SE elliptical, funnel-shaped sill with a maximum thickness of <1000 m in the inner domain, decreasing to <400 m close to the exposed contacts with the metamorphic basement (i.e., Casini et al., 2025). Geochemistry and field structural analysis highlights three different magmatic units (MU_{1-3}) that represent the roof of the pluton (MU_1), the wall-core domain (MU_2), and the transition from the core to the floor of the intrusion (MU_3), respectively (Fig. 11a). The contacts between the different magmatic units are generally gradational over tens to hundreds of meters. Close to the margins of the pluton and in proximity of its roof, the contacts instead become sharper and are sometimes marked by thin (<0.5 m) aplitic dykes parallel to the magmatic foliation (Fig. 11b). The MU_1 unit is exposed in the SE quadrant of the pluton and consists of fine-grained muscovite-bearing leuco-monzogranite with a biotite content generally lower than 10 vol.%, and globular quartz. Sporadic and relatively small (<5 cm-long) idiomorphic K-feldspar phenocrysts mark a weak magmatic foliation gently dipping toward E or SE. A swarm of sub-vertical pegmatitic and aplitic dykes, sometimes rich in garnet and cordierite, emplaced close to the NW border of the pluton; it has been interpreted as part of this magmatic unit (Cuccuru et al., 2018). The roof of the pluton overlies a strongly porphyritic, medium-grained, monzogranite with an average grain size of about 2 cm, labelled as MU_2, that represents a more internal domain of the magmatic chamber (Cuccuru et al., 2018). MU_2 is characterised by a variable biotite content between 15 and 25 vol.% and abundant K-feldspar megacrysts up to 20 cm-long (Fig. 11c). Small micro-granular mafic enclaves of mostly trondhjemitic to granodioritic composition and fragments of metamorphic xenoliths are occasionally present, particularly close to the contacts with MU_3 and MU_1 units. These, together with the K-feldspar megacrysts, define a strong magmatic foliation oriented roughly NW-SE or and moderately dipping toward the pluton borders (Fig. 11a). The MU_3 unit is a medium-grained biotite monzogranite quite similar to MU_2, except for the abundance of biotite schlieren, fine-grained mafic enclaves and metamorphic xenoliths. Large K-feldspar megacrysts are more common than within the MU_2 unit, commonly forming cumulitic domains with a complex 3D shape, ranging from tabular to stretched conic, to pipe-like structures (Fig. 11d).

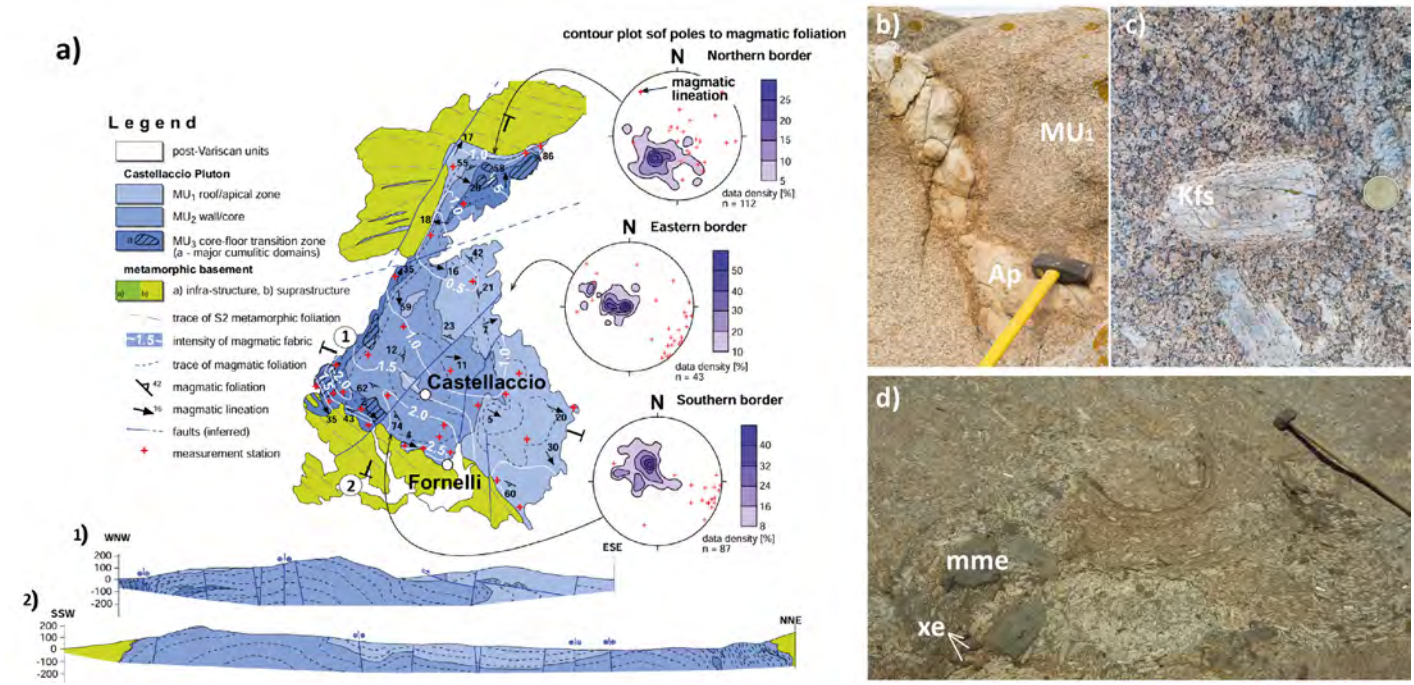

Fig. 11 - Field structural characteristics of the Castellaccio Pluton: a) structural-geological map of the pluton (modified from Casini et al., 2025) showing the different magmatic units (MU_1-MU_3) and the pattern of magmatic flow foliation (black dashed lines). The orientation of magmatic foliation and lineation is also shown in stereographic projections to the right of the map (lower hemisphere, equal area Schmidt's projection); b) aplitic dykes injected with plastic contacts within the roof-apical zone of the pluton (MU_1 magmatic unit); c) close-up of a large K-feldspar phenocryst (Kfs) in the wall-core domain of the pluton (MU_2 magmatic unit); d) aspect of K-feldspar-rich cumulitic domains common within the wall-floor transition zone of the pluton (MU_3 magmatic unit).

COMPOSITION AND GEOCHEMICAL ZONATION

The pluton is composed of felsic rocks with SiO_2 contents ranging from 61.60 to 78.23 wt.% (Casini et al., 2025; Idini et al., 2025). The major-elements composition of MU_1 and MU_2 magmatic units largely overlaps as most samples can be classified as granites or monzogranites (Debon & Le Fort, 1988), whereas MU_3 samples plot into the tonalite to monzogranite fields (Fig. 12a). The different magmatic units exhibit an overall ferroan-magnesian transitional character defining a classical calc-alkaline trend in the Modified Alkali-Lime diagram (Fig. 12b). The FeO+MgO content is always negatively correlated with the A/CNK (Casini et al., 2025), and Zr (18-301 ppm) is apparently uncorrelated with Ba and negatively correlated with SiO_2 (Fig. 12c). The distribution of major and trace elements is somewhat heterogeneous through the pluton, evidencing distinctive patterns in the northern-western sector, central, and south-eastern domains. The SiO_2 content (Fig. 12d) is maximum in the eastern and south-eastern part of the pluton which corresponds to the roof zone (i.e., Cuccuru et al., 2018; Casini et al., 2025). The distribution of Zr is nearly antithetical to that of SiO_2 reaching the lowest values in the eastern and southern margins of the pluton, whereas a localised Zr positive anomaly with values reaching 280-290 ppm appears in the northwestern sector of the pluton in correspondence of the pluton core MU_2 (Fig. 12e). The pattern of A/CNK is similar to that of silica (Fig. 12f).

PETROGRAPHY AND MICROSTRUCTURES

The dominant MU_2 and MU_3 rocks are strongly porphyritic, with a medium-grained matrix and large, up to 20 cm-long, K-feldspar megacrysts (Fig. 11c). The matrix consists of quartz + plagioclase + biotite + small interstitial K-feldspar grains (Fig. 13a). Common accessory minerals include zircon + apatite + ilmenite + titanite ± monazite. The K-feldspar and plagioclase megacrysts are generally idiomorphic and show no evidence of plastic deformation, except within cumulitic domains where they occasionally show zonal undulous extinction and rare subgrains (Fig. 13a). The megacrysts are frequently perthitic and contain abundant inclusions of sub-idiomorphic plagioclase, quartz and biotite, and several accessory phases. Plagioclase and quartz in the matrix preserve evidence for extensive sub-magmatic deformation (Fig. 13b) such as intra-crystalline fractures filled by quartz + albitic plagioclase + muscovite (Bouchez et al., 1992; Paterson et al., 1989; 1998; Vernon et al., 2004; Casini et al., 2025) and chessboard pattern (i.e., Kruhl, 1996; Peng and Redfern, 2013; Casini et al., 2025; Pieruccioni et al., 2025).

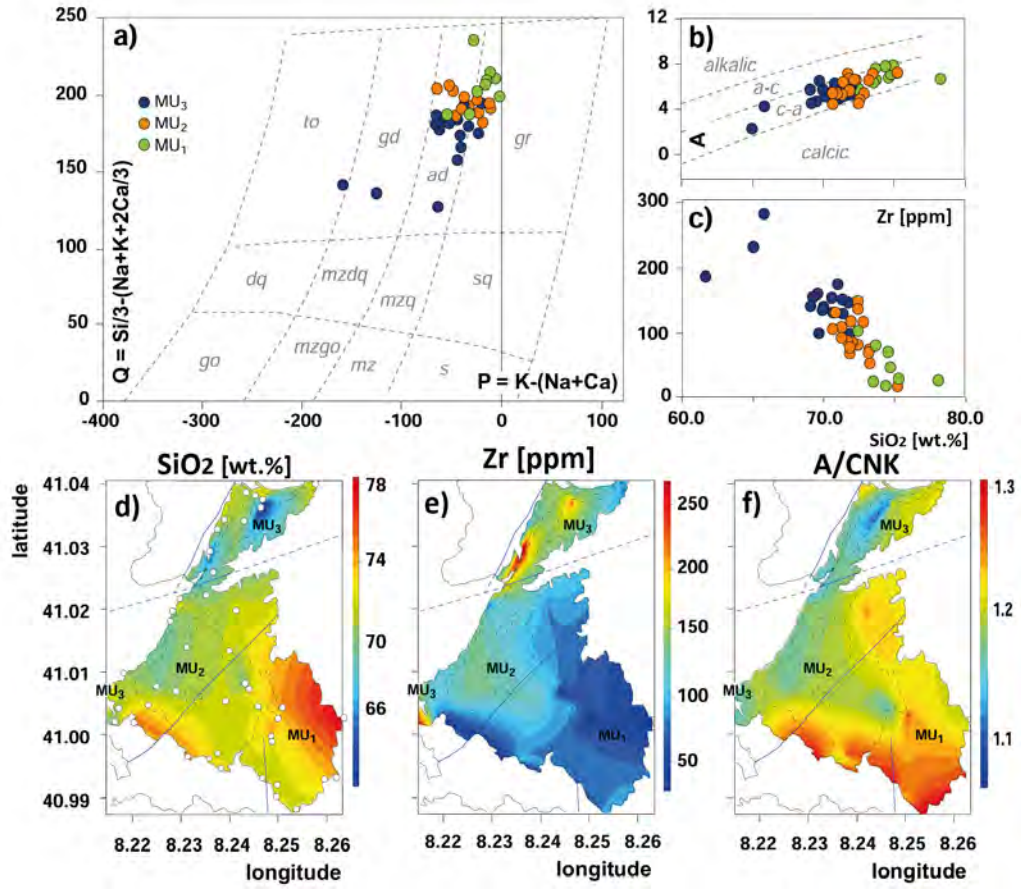

Fig. 12 - Geochemistry of the three magmatic units of the Castellaccio Pluton (modified from Casini et al., 2025): a) major-element classification (Debon & Le Fort, 1988), gr – granite, mzg – monzogranite, mz – monzonite, go – gabbro, gd – granodiorite, to – tonalite, ad – adamellite, dq – quartz-diorite, mzdq – quartz monzodiorite, quartz-monzogabbro, mzgo – monzogabbro, monzodiorite, mzq – quartz-monzonite, sq – quartz-syenite; b) Modified Alkali-Lime diagram (Frost & Frost, 2008), c) Harker variation diagram showing the content of Zr in relation to SiO_2; d) pattern of SiO_2, the white circles indicate the position of samples selected for bulk chemical composition; e) distribution of Zr; f) variation of A/CNK ratio.

https://doi.org/10.3301/GFT.2026.02

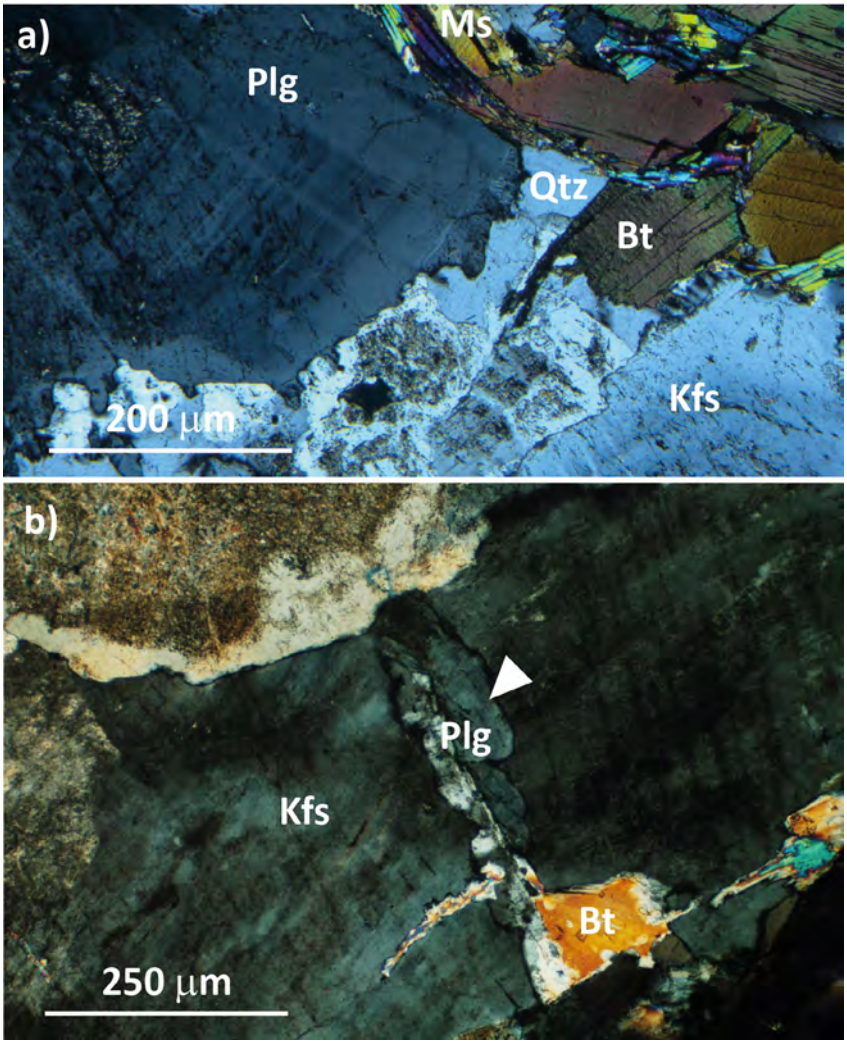

Fig. 13 - Microstructure of MU_2 rocks: a) typical matrix assemblage of phenocryst-poor domains composed of plagioclase with normal zonation, fine-grained and sub-idiomorphic K-feldspar, anhedral quartz, biotite and muscovite. Note the weakly developed cuspate grain boundaries at the contact between plagioclase and quartz, K-feldspar; b) sub-magmatic fracture (white arrow) filled with albitic plagioclase + quartz + biotite cutting through a small K-feldspar phenocryst.

Stop 2.1 - Andalusite hornfels along the northern border zone

Coordinates: Lat. 41°02'48"N, Long. 8°14'46"E
Location: Punta Sa Nave (Asinara, SS)

This outcrop is about 1 km to the south of stop 1.4 and can be reached from the road by walking for a few meters on rough terrain on the steep slope that goes down to the western coast of the island (Fig. 1b). Stop 2.1 exposes a thick sequence of paragneiss and micaschists alternating with quartz veins and large (5-50 cm-thick) andalusite-rich layers. The rocks show clear structural relationships between the S_1/S_2 foliations, the transposed bedding still recognizable in the hinge zone of some F_2 folds (S_0), and the late F_3 folds. The latter are upright open folds often associated to kink bands and brittle-ductile shear zones developed under retrograde sub-greenschist facies conditions, as testified by the weak chlorite + epidote spaced cleavage. The mineral assemblage of paragneiss is characterised by andalusite + biotite + plagioclase + quartz ± muscovite ± staurolite. As observed in the garnet-bearing micaschists of stop 1.3, staurolite is only preserved as partly corroded inclusion within andalusite porphyroblasts. Zircon, monazite and tourmaline are common accessory minerals. Thin (5-50 cm-thick) andalusite-bearing quartz veins and quartz + andalusite ± K-feldspar pegmatitic dykes are widespread throughout the outcrop. Quartz veins are mostly parallel to the regional S_2 schistosity. However, andalusite-bearing veins and pegmatite dykes cut through the S_1/S_2 foliation, suggesting that HT-LP metamorphism and magmatic activity post-date the phase of regional shortening (i.e., Carmignani et al., 1994; Carosi et al., 2004; Rossi et al., 2009).

Stop 2.2 - K-feldspar cumulates and flow structures in the wall-roof transition zone

Coordinates: Lat. 41°02'21"N, Long. 8°15'23"E
Location: Tumbarino-Punta l'Arroccu (Asinara, SS)

The itinerary continues moving southward on the road until the Tumbarino village. The outcrop can be reached by walking along an easy footpath (about 1.5 km) that goes from Tumbarino toward east-northeast by the sea (Fig. 1b).

https://doi.org/10.3301/GFT.2026.02

The path goes through a nearly continuous outcrop of MU_2 rocks with small MU_3 domains rich in K-feldspar cumulates, offering a spectacular view on the pluton wall/floor transition zone (Fig. 14a). The dominant rock type is a porphyritic coarse-grained peraluminous granite, locally grading to granodiorite, composed of quartz + K-feldspar + An_{20-25} plagioclase + biotite + muscovite. Zircon, titanite, ilmenite, tourmaline and apatite are common accessory minerals. Several magmatic structures related to the flow of the crystal mush during incremental construction of the pluton by multiple injections of magma (i.e., Casini et al., 2025) can be observed, such as: i) ring schlieren, ii) compositional banding, iii) partly assimilated metamorphic xenoliths, iv) tiled K-feldspar and plagioclase phenocrysts, and v) a variety of ladder dykes ranging from a few cm to tens of m (Fig. 14b). These dykes are frequently made of large K-feldspar megacrysts that locally cluster forming cumulitic domains composed of up to 80 vol.% of K-feldspar (Fig. 14c). The cumulitic domains commonly form steep funnel- or pipe-like structures, sometimes tapering downward, but transitional and more complex geometries occur as well. Based on geochemical arguments, microstructural observation and mineralogical analysis, it has been proposed that K-feldspar megacrysts formed relatively early during the solidification of the Castellaccio Pluton, when the system was still dominated by melt (Idini et al., 2025). The proposed sequence of crystallisation and the overall sub-vertical orientation of funnel-shaped cumulitic domains suggest that these structures may have formed because of Rayleigh-Taylor instability and convective overturn of the earlier magma batches during incremental growth of the pluton (i.e., Casini et al., 2025).

Stop 2.3 - The chilled margin in the southern border zone

Coordinates: Lat. 41°00'01"N, Long. 8°13'17"E
Location: Fornelli Lake (Asinara, SS)

The chilled margin of the pluton is well exposed along the dirty road going from the now dismissed Fornelli maximum security prison toward the western coast of Asinara, a few hundred meters after the dam (Fig. 1b). The contact between the oligoclase + garnet bearing paragneisses and the granite is sharp and mostly dipping towards S-SW. Within 5-10 m from the contact, the granite shows a very fine average grain size between 1-5 mm and several features suggestive of rapid cooling, such as globular quartz, microcrystalline domains, and small mm-sized partly disaggregated metamorphic xenoliths (Fig. 15a). These features have been interpreted in terms of rapid

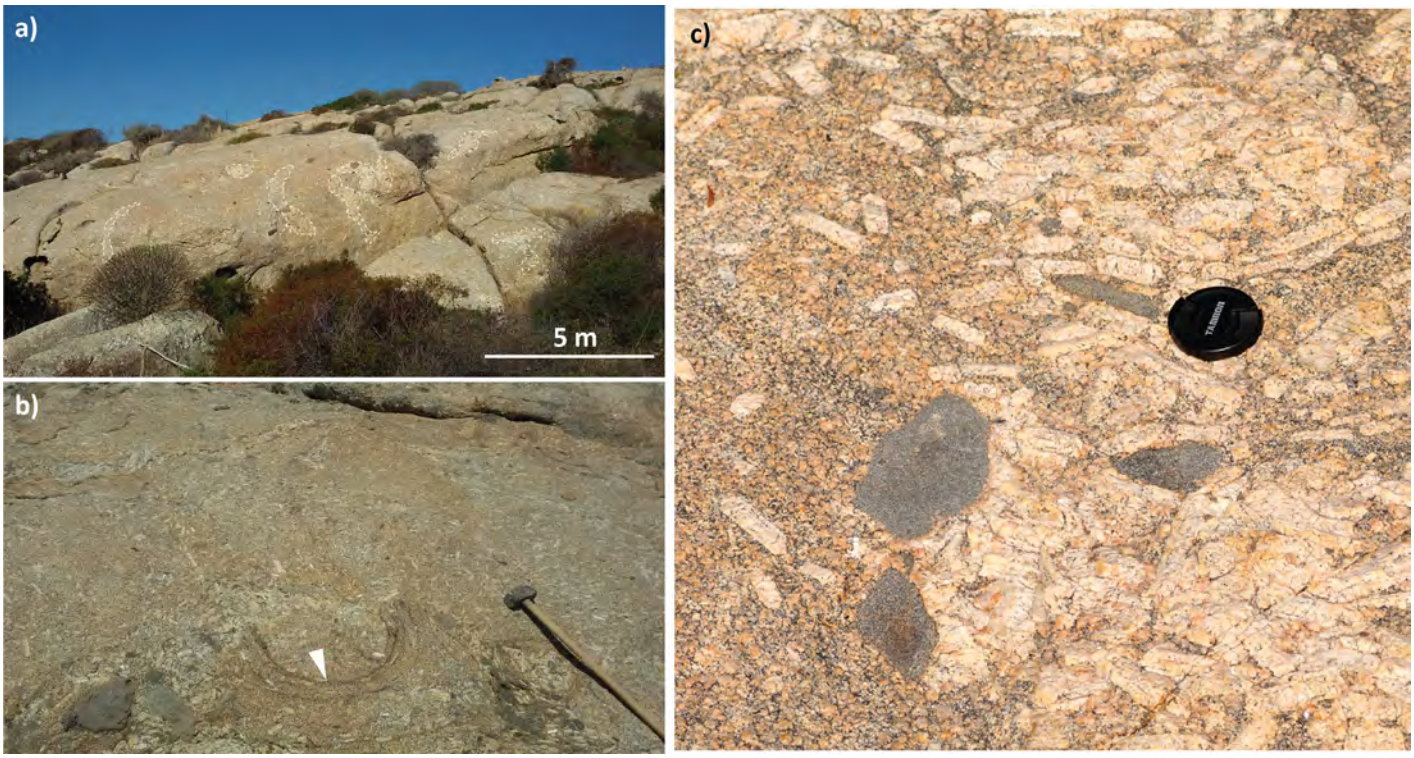

Fig. 14 - Structure of the MU_2/MU_3 units: a) outcrop of MU_2 unit close to the Pta Marcutza site, the white dashed lines mark the K-feldspar-rich cumulitic domains; b) Kfeldpar cumulate, the white arrow mark ring schlieren forming a ladder dyke structure; c) close up of a Kfeldpar-rich cumulitic domain.

cooling in response to a large temperature difference between the melt and the host rock (i.e., Cuccuru et al., 2018; Casini et al., 2025). K-feldspar phenocrysts are rarely observed within the chilled margin and, where present, are generally small (< 5cm). Going toward the interior of the pluton, the chilled margin passes sideways to the typical MU_2 unit characterised by large K-feldspar megacrysts, sometimes forming 10-100 m-thick cumulitic domains. The transition between the chilled margin and MU_2 is gradational, with discontinuous bands of fine-grained granite and micro-granite alternating to porphyritic monzogranite (Fig. 15b).

Stop 2.4 - Aplitic and granitic dykes

Coordinates: Lat. 41°00'07"N, Long. 8°12'42"E
Location: Punta Pedra Bianca (Asinara, SS)

The Punta Pedra Bianca cliff provides a spectacular view of the contact zone between the metamorphic basement and the external part of the pluton. The outcrop can be reached from stop 2.3 following the dirty road toward northwest for about 500 meters, until a sharp hairpin near a huge rocky cliff (Fig. 1b). The pluton consists of several granitic and aplitic dykes and sills (0.1-10m thick) showing complex crosscutting relationships that represent different magma batches of variable thickness (Fig. 15c; Cuccuru et al., 2018; Casini et al., 2025). Notably, the grain size of granitic bodies is also extremely variable from nearly glassy or very fine-grained to medium-grained, without any obvious correlation with the size of the magmatic batch (Fig. 15d). These observations have been interpreted in terms of competition between progressive heating of the metamorphic country rock and variable magma influx rate during the incremental build-up of the granitic body (i.e., Casini et al., 2025; Idini et al., 2025). Despite minor textural differences due to grain-size variation and the occasional presence of K-feldspar phenocrysts, the composition of the granite is overall similar to the MU_1-MU_2 units and consists of quartz + K-feldspar + plagioclase + biotite + muscovite ± garnet ± tourmaline.

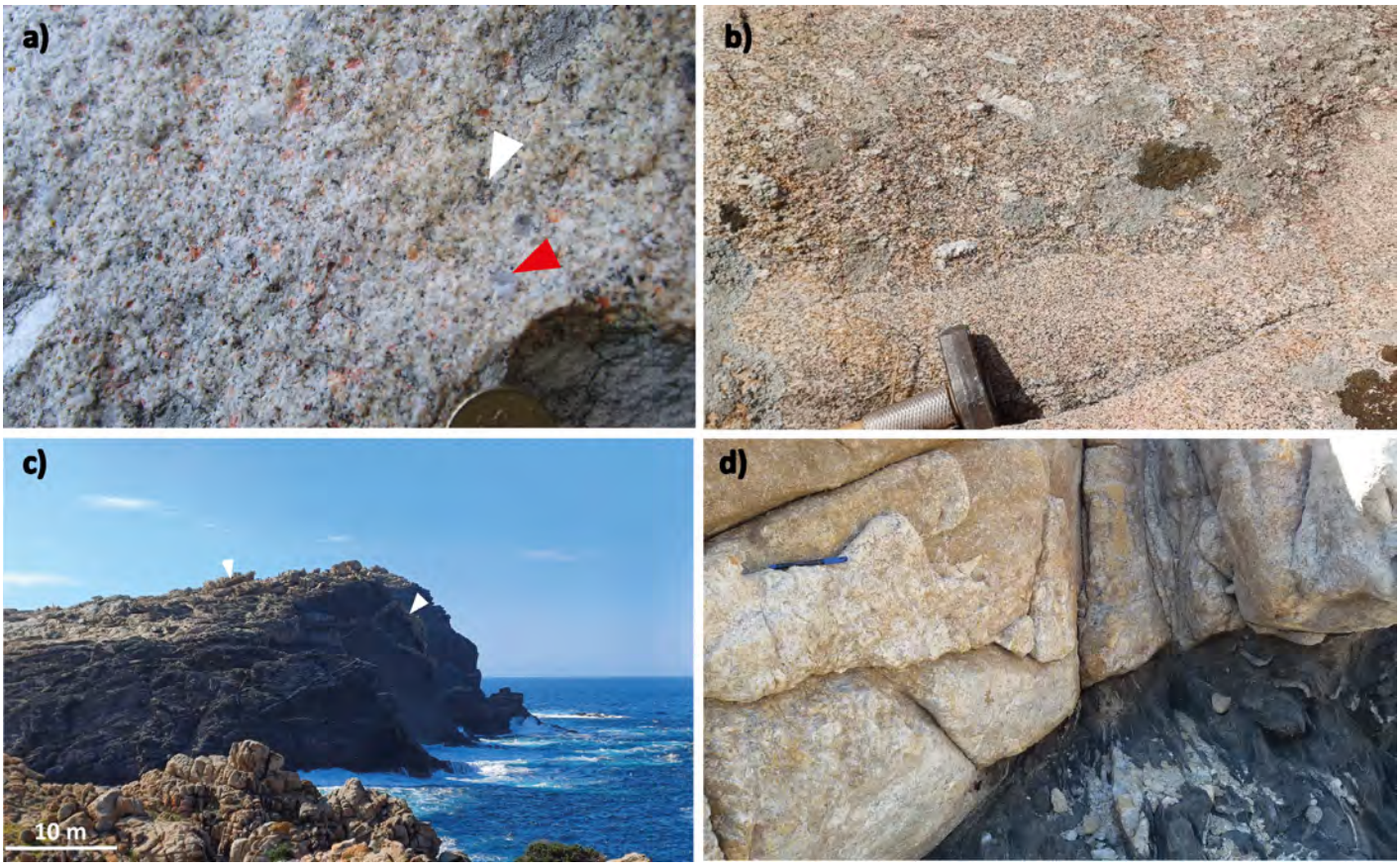

Fig. 15 - The chilled margin of the Castellaccio Pluton: a) close-up of a micro-granitic layer rich in small mm-sized metamorphic xenoliths (white arrow) and globular quartz domains (red arrow), about 1.5 cm coin for scale; b) sharp contact between a medium to coarse-grained porphyritic granite and a very fine-grained equigranular granite; c) overview of the border zone showing several aplitic, pegmatitic and granitic dykes and sills (white arrow) intruding the metamorphic basement, d) close-up of the contact between an aplitic sill and the metamorphic basement.

DAY 3

THE MIGMATITIC COMPLEX

The third day is entirely dedicated to the migmatitic complex of Punta Bianca and to the Barrabisa peraluminous pluton (Fig. 16). All the outcrops proposed in this part of the field trip (stops 3.1-3.4) can be reached from the beach of Lu Polthiddolu village, walking for 10-30 minutes on a small footpath that goes toward west and northwest through the rocky cliff by the sea (Fig. 1c). The Barrabisa pluton is a ribbon-like syntectonic S-type strongly peraluminous andalusite + cordierite-bearing granodiorite injected within a 1-4 km-wide E-W late-Variscan shear zone (Casini et al., 2015b; De Luca et al., 2023). In the Punta Bianca locality, object of stops 3.1-3.4, the Barrabisa shear zone deforms early Variscan migmatites (360-340 Ma; Giacomini et al., 2006, 2008; Casini et al., 2023), well exposed in polished wavecut platforms along a rocky cliff accessible through an easy walk. Due to extremely favorable conditions of exposure, the outcrops offer the opportunity of investigating the 3D architecture of melt pathways from migmatites to the roots of the syntectonic pluton, and the mechanism of melt extraction/migration. The migmatitic massif consists of melt-poor metatexite (melt 5-20 vol.%), diatexite (melt 20-40 vol.% on average, locally reaching 80-90 vol.%), and rare amphibolite boudins (Fig. 16b). These latter are compositionally monotonic rocks with hornblende + plagioclase ± titanite ± ilmenite as common mineral assemblage. Metatexite is composed of quartz + biotite + plagioclase + K-feldspar ± sillimanite and muscovite is present only as a secondary phase replacing K-feldspar or plagioclase. The geochemical fingerprint of metatexite includes negative εNd values generally lower than -5, highly radiogenic $^{87}Sr/^{86}Sr$ ratio between 0.709-0.712 (i.e., Casini et al., 2015a) and abundant inherited zircon grains with clear magmatic oscillatory zoning. This indicates that metatexites are primarily derived from Ordovician calc-alkaline orthogneisses, with only a minor component of metasediments and amphibolite of unknown age (i.e., Cruciani et al., 2008; Casini et al., 2015b; Casini et al., 2023). On the contrary, diatexites are quartz + K-feldspar

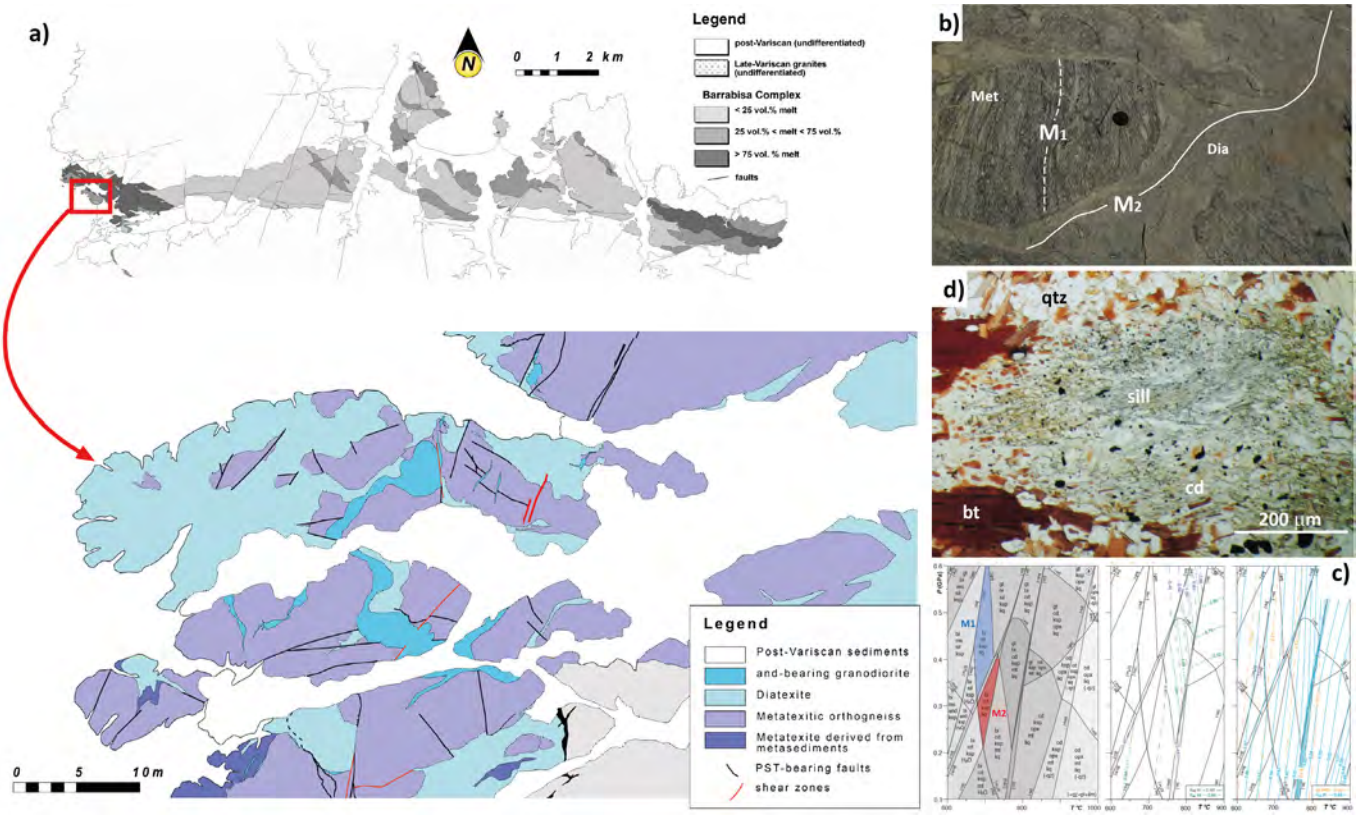

Fig. 16 - The Punta Bianca migmatitic complex and the Barrabisa Pluton: a) simplified structural model of N Sardinia showing the main migmatitic outcrops, Permian and Carboniferous plutons of the Corsica-Sardinia Batholith including the peraluminous Barrabisa Pluton; b) representative outcrop of migmatite showing the field relationships between metatexite (Met) and diatexite (Dia), M_1 and M_2 indicate the first generation of leucosomes of early Carboniferous age and the second, HT-LP generation of leucosomes, respectively; c) pseudosection of metapelic metatexite showing the PT field of the two melting stages (modified from Casini et al., 2023); d) photomicrograph of a metapelitic metatexite showing replacement of sillimanite + biotite + quartz by cordierite during typical decompression under near isothermal HT conditions.

+ plagioclase + biotite + garnet ± cordierite ± andalusite migmatites apparently derived from low-pressure melting of Al_2O_3-poor metasediments. The peculiarity of the Punta Bianca migmatitic massif is the clear preservation of at least two distinct melting stages reflecting the switch from anhydrous muscovite-dehydration melting to water-fluxed melting during decompression (Fig. 18a). The first melting stage M_1 recorded by metatexite involves dehydration melting of muscovite at a minimum pressure of ~0.45 GPa and 720-740°C (Fig. 16c; Casini et al., 2023). The age of the M_1 stage is not precisely constrained because of extensive resetting of all isotopic systems during the subsequent melting stage M_2; yet a few zircons preserve a lower Carboniferous age which is consistent with the regional dataset (Ferrara et al., 1978; Di Vincenzo et al., 2004; Giacomini et al., 2006). Cordierite overgrowths replacing sillimanite in metapelitic migmatite, combined with the composition of plagioclase and K-feldspar, indicates decompression to ~0.3 GPa after M_1 (Fig. 16d). This interpretation is consistent with the dense network of pseudotachylyte-bearing faults deforming the M_1 fabric (Fig. 17), suggesting cooling to greenschist-facies conditions before the onset of the second melting stage M_2 (< 500°C). Pseudosection modelling of metatexite and diatexite provide consistent results supportive of nearly isobaric re-

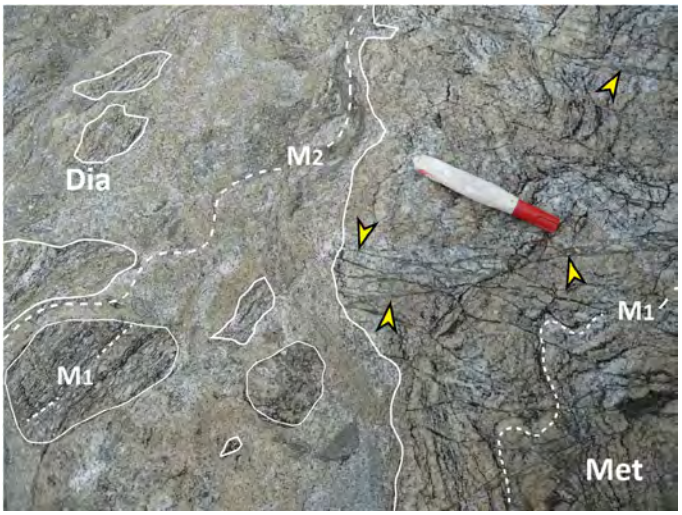

Fig. 17 - Contact between diatexite (Dia) with small fragments of metatexite preserving the M_1 fabric and the metatexitic orthogneiss (Met); the magmatic fabric M_2 of diatexite is shown. The yellow arrows indicate a set of large pseudotachylyte deforming the M_1 fabric of the orthogneiss, but not the M_2 fabric of diatexite.

heating up to ~750°C leading to fluid-fluxed melting during M_2, followed by further cooling below the solidus (Casini et al., 2023). The inferred P–T-d path of the migmatitic massif (Fig. 18) is consistent with decompression and cooling of

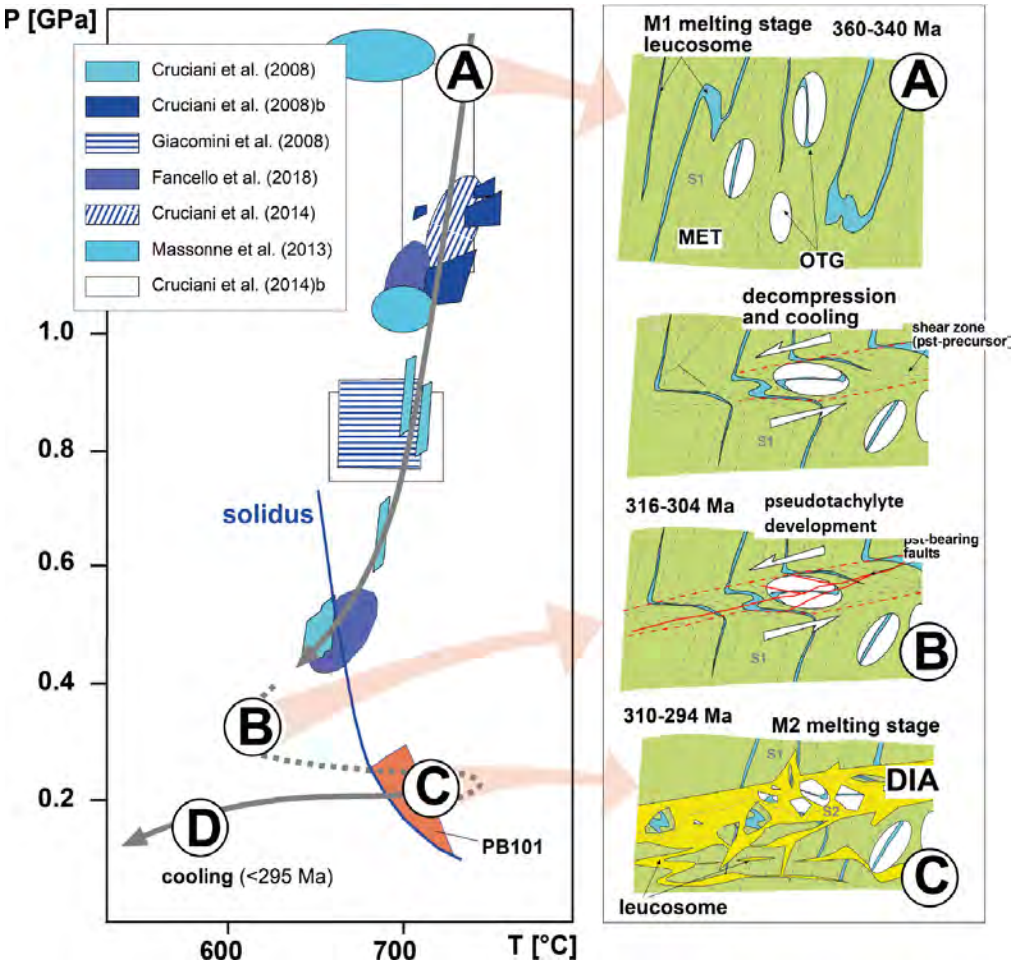

Fig. 18 - Conceptual model of partial melting and structure development in the Punta Bianca migmatitic massif. In the left panel, PTt path of Punta bianca migmatites integrated with data from nearby metamorphic massifs of N Sardinia and southern Corsica. In the right panels, sequence of metamorphic and deformation stages recorded by Punta Bianca migmatites during post-orogenic decompression of the Variscan crust.

the Variscan crust through post-collisional extension and collapse of the thickened orogenic crust, followed by nearly isobaric re-heating and re-hydration at low pressures (~0.3 GPa). U/Th-Pb monazite ages indicate an upper bound of 310-316 Ma for the second melting stage, suggesting that M_2 is coincident with the regional phase of crustal shearing and the onset of U_2 magmatism. The cause of the local increase of temperature and fluid availability during M_2 is still unknown, but likely requires magmatic underplating possibly combined with focused shear heating (Maino et al., 2015; Casini et al., 2015b).

Stop 3.1 - Garnet-bearing diatexite and amphibolite

Coordinates: Lat. 41°10'59", Long. N 9°09'42"E
Location: Punta Bianca (Lu Polthiddolu, SS)

The first stop of day 3 provides an exceptional 3D view of the geometry of the migmatitic massif and the relationships between the various types of migmatite, and can be reached by an easy 10-minute walk following the footpath by the sea starting from the northern side of Lu Pulthiddolu beach (Fig. 1c). The outcrop consists of garnet-bearing diatexites related to the second, LP, melting stage M_2. Diatexite contain fragments of compositionally diverse metatexites and amphibolite boudins, ranging from biotite + sillimanite-rich rocks apparently derived from metapelites to quartz + plagioclase + biotite fragments with occasional idiomorphic K-feldspar porphyroclasts that have been interpreted as relics of Ordovician orthogneiss (Cruciani et al., 2008; Oggiano et al., 2010; Casini et al., 2023). Diatexite in this outcrop has high melt proportion between 40 to 80% and shows a dominantly magmatic fabric due to the shape preferred orientation of plagioclase crystals and biotite and by compositional layering marked by garnet and biotite-rich bands alternating with quartz + plagioclase-rich domains (Fig. 19). The magmatic foliation is usually steep and strikes E-W to WNW-ESE, nearly parallel to the elongation of the Barrabisa Pluton and at low angle to the regional S_2 foliation (Fig. 16a). These observations suggest the M_2 melting stage is likely related to the D_2 transpressional phase (i.e., Carosi et al., 2004; Di Vincenzo et al, 2004; Casini et al., 2023).
The amphibolite boudins are fine-grained rocks characterised by a poorly diagnostic hornblende + plagioclase assemblage, but show relics of an early (M_1?) HT fabric which is usually at high-angle relative to the dominant M_2 fabric of diatexite. Locally amphibolite boudins are heavily fractured and injected by M_2 melts.

Stop 3.2 - Amphibole-bearing granodiorite (Punta Bianca, SS)

Coordinates: Lat. 41°10'59"N, Long. 9°09'38"E
Location: Punta Bianca (Lu Polthiddolu, SS)

Stop 3.2 can be reached following the footpath by the sea toward west for about 80 meters, until a stretch of winding footpath that goes uphill. Here, diatexite similar to that of stop 3.1 includes fragments of a fine-grained, darkish, amphibole-bearing granodiorite composed of andesinic plagioclase + Mg-hornblende + biotite + quartz ± apatite. The larger fragments (1-2 m wide) are usually angular

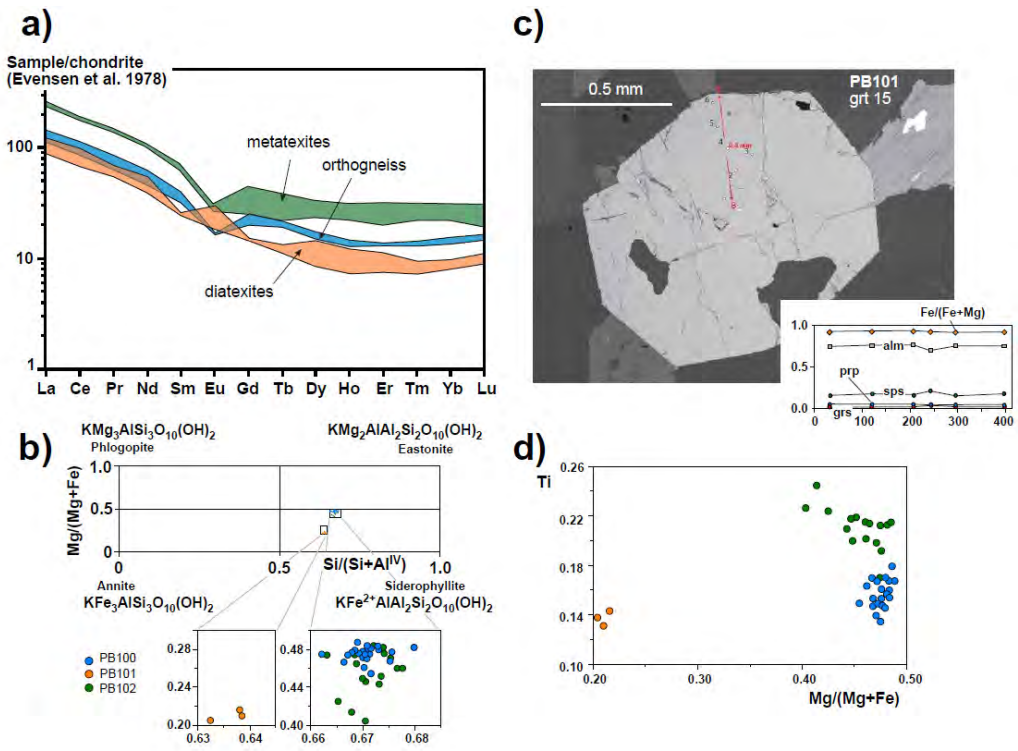

Fig. 19 - Geochemical and compositional data of migmatites from the Punta Bianca massif: a) cumulative REE patterns of different migmatite types; b) composition of biotite; c) representative compositional profile of garnet from diatexite, d) Ti content of biotite of all samples (modified from Casini et al., 2023).

forming sharp contacts with the host diatexite; however, smaller fragments are more rounded and the contacts with the host are locally gradational testifying limited diffusion. The microstructure of the granodiorite is characterised by idiomorphic plagioclase with oscillatory zoning, sub-idiomorphic to idiomorphic amphibole partly replaced by biotite, and interstitial quartz (Fig. 20a, b). Although the age of granodiorite is still unknown, all minerals show little evidence for internal lattice strain suggesting a purely magmatic evolution, thus the mafic magmatism should be almost contemporaneous with the second melting stage M_2, and not inherited from a pre-Variscan magmatic event.

Pseudosection modeling in the KNCFMASHTOCr system (Green et al., 2016) indicates that the granodiorite melt started crystallizing An_{75} plagioclase at about 1050°C in the pressure range of 0.25-0.45 GPa, whereas amphibole and An_{55-60} plagioclase formed at a lower temperature close to the solidus, around 800-820°C (Fig. 20c). The activity of H_2O calculated close to the solidus ranges between 0.35 and 0.6 at about 0.3 GPa. When considered together, these results indicate that the granodiorite fragments enclosed within the diatexite likely represent a relatively hot, hydrous mafic melt.

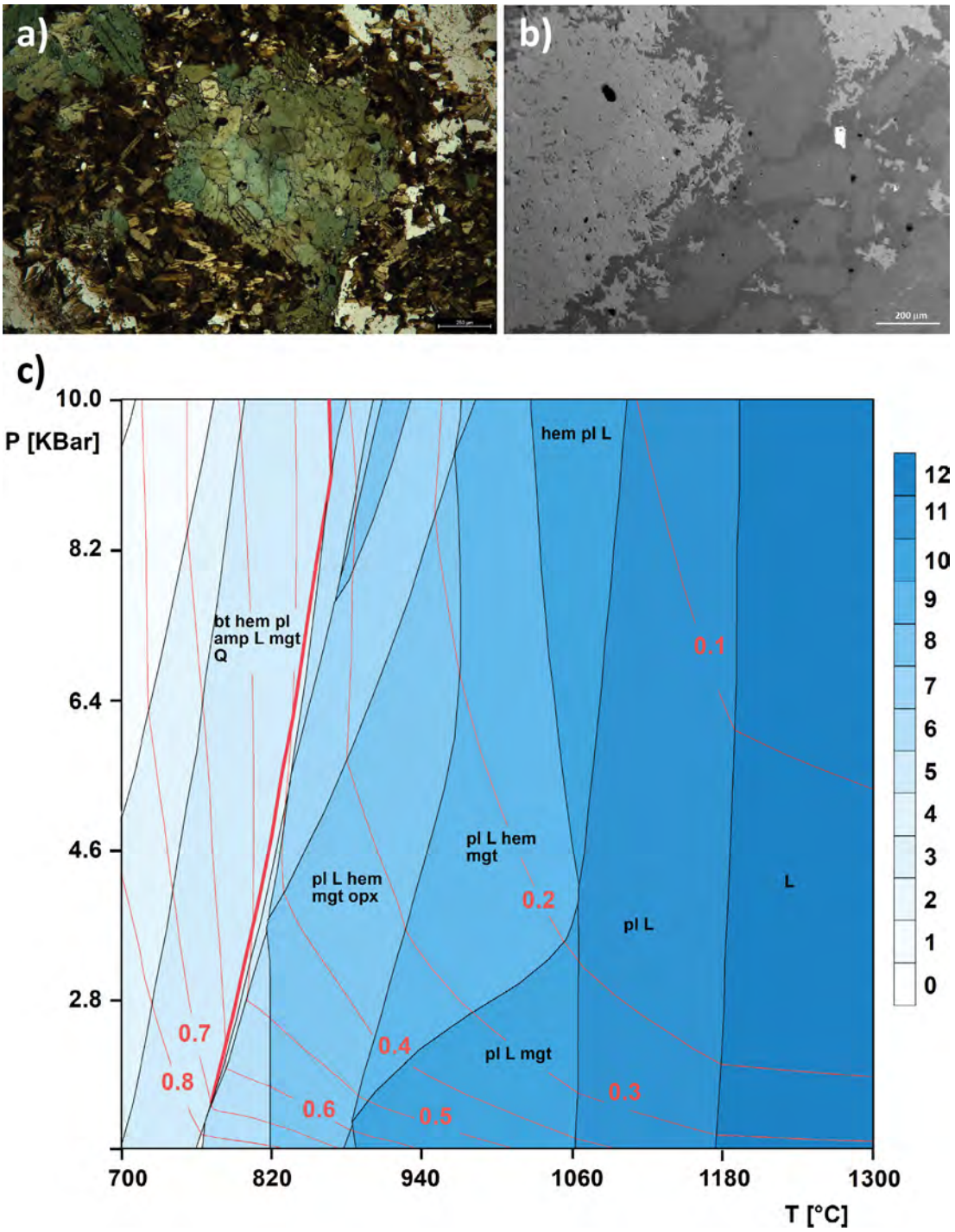

Fig. 20 - Microstructure and composition of amphibole-bearing granodiorite from the Pta Bianca migmatitic massif: a) biotite rim around amphibole (Mg-hornblende); b) SEM image of amphibole partly replaced by biotite in a groundmass of andesinic idiomorphic plagioclase and quartz; c) pseudosection of amphibole-bearing granodiorite showing the stability field of amphibole (lower-T side of the thick red line) and H_2O isopleths (thin red lines). The pseudosection has been calculated using the MAGEmin software (Riel et al., 2022).

https://doi.org/10.3301/GFT.2026.02

Stop 3.3 - Co-seismic deformation structures related to water-fluxed melting (Punta Bianca, SS)

Coordinates: Lat. 41°11'07"N, Long. 9°09'32"E
Location: Punta Bianca (Lu Polthiddolu, SS)

The outcrop can be reached following the footpath uphill until a flat, then taking the right for about 30 meters to a wooden ladder that allow climbing the dry-stone wall. Continue on the footpath through bushes and small meadows toward north up to the second rough descent that takes to the sea, about 180 meters from the dry-stone wall. Stop 3.3 is just a the end of the descent, in a very narrow bay oriented E-W that resembles a miniature fjord (Fig. 1b). The outcrop offers an excellent 3D view of the geological structure of the migmatitic massif due to well-polished outcrops and good lateral continuity. The central part of the outcrop consists of metatexite derived from a coarse-grained granodioritic orthogneiss, sometimes preserving big K-feldspar porphyroclasts, set within M_2 diatexites. Metatexite preserves an old migmatitic fabric related to the M_1 melting stage, which has been correlated to the early Carboniferous phase of D1 shortening (i.e., Ferrara et al., 1978; Giacomini et al., 2005, 2006; Casini et al., 2023). The boundaries between metatexite and diatexite are usually sharp and often decorated by angular fragments of orthogneiss, which are only partly assimilated by the M_2 diatexitic melt. Metatexite derived from magmatic protoliths preserves thin (0.5 – 2 cm-thick) quartz + plagioclase + biotite ± K-feldspar M_1 leucosomes, locally folded by tight to isoclinal asymmetric folds and sub-vertical shear zones. A few fragments of metatexite derived from metapelitic protoliths can also be observed in the south-western part of the bay. These rocks consist of 10-15 vol.% of cm-thick quartz + plagioclase + K-feldspar leucosomes set within a biotite-rich melanosome composed of quartz + biotite + plagioclase + K-feldspar + sillimanite ± cordierite. Zircon, monazite, allanite and apatite are common accessory minerals. Small garnet can be occasionally present within the melanosome (Giacomini et al, 2006). Metatexite fragments are set within the diatexite. These are melt-rich migmatites similar to that observed in stop 3.1, consisting of M_2 melt composed of quartz + plagioclase + K-feldspar + biotite + garnet, and variable proportions of restitic fragments of metapelitic metatexite, amphibolite and migmatitic orthogneiss. Zircon, apatite and monazite are normally present as accessory phases, altogether with cordierite. A dense network of tiny (0.1 – 1.0 cm-thick) fractures and pseudotachylyte-bearing faults offset the M_1 fabric of metatexitic orthogneiss, but not diatexite (M_2), thus establishing a clear relative chronology (Fig. 21a,b). Fractures and pseudotachylyte-bearing faults are mostly steep and oriented NE-SW and NNW-SSE, however a few gently dipping faults with E-W orientation occur (Fig. 16a). At places, typically close to the contact between the metatexitic orthogneiss and diatexite, faults pass sideways to melt-bearing ductile shear zones injected by M_2 melts of diatexite. U/Th-Pb dating of monazite within the metapelitic metatexite indicates that M_1 should be early Carboniferous (337±12 Ma; Casini et al., 2023), as generally observed in other migmatitic massifs of northern Sardinia and southern Corsica (Ferrara et al., 1978; Giacomini et al., 2006, 2008). U-Pb dating of small, prismatic, zircon crystals micro-sampled within pseudotachylyte veins provided consistent, though statistically weak, results supportive of a Mississippian-early Pennsylvanian age (320-310 Ma) of the seismic event (Casini et al., 2023). On the contrary, the Carboniferous ages (303–313 Ma; Fig. 21c,d) preserved within the metatexitic orthogneiss would reflect the thermal peak of M_2 nearly coeval with the onset of U_2 magmatism in the Corsica-Sardinia Batholith (Casini et al., 2012, 2015a,b, 2023).

Stop 3.4 - Contact between S. Teresa monzogranite and the Barrabisa pluton

Coordinates: Lat. 41°11'16"N, Long. 9°09'40"E
Location: Punta Bianca (Lu Polthiddolu, SS)

The last outcrop of the day can be reached going back uphill to the start of the descent, then following the footpath toward north through low bushes and rocky meadows for about 200 meters up to a dry-stone with another wooden ladder. After climbing the wall, continue to the north for about 150 meters in direction of a huge rocky cliff by the sea. The stop 3.4 is just on the small rocky beach a few meters from the cliff. Here, the migmatitic complex passes laterally to the late Carboniferous S. Teresa pluton (307 Ma +4/-6; Oggiano et al., 2005; Casini et al., 2015b). The contact strikes roughly E-W and is steeply dipping toward the south. The granite is a porphyritic medium-grained biotite granodiorite with relatively small (4-6 cm), brown to pinkish, idiomorphic K-feldspar phenocrysts locally oriented parallel to the contact. However, magmatic fabric is poorly developed. The pluton does not show any significant grain-size reduction close to the migmatites, indicating little temperature difference between the magma and the host rocks. All these observations suggest that migmatites were likely still close to the solidus during the emplacement of the pluton. A 1-2 m-wide band of apparently undeformed micro-granular mafic enclaves (5 – 50 cm-wide), mostly tonalites or amphibole-bearing micro-granodiorite, can be observed close to the contact.

https://doi.org/10.3301/GFT.2026.02

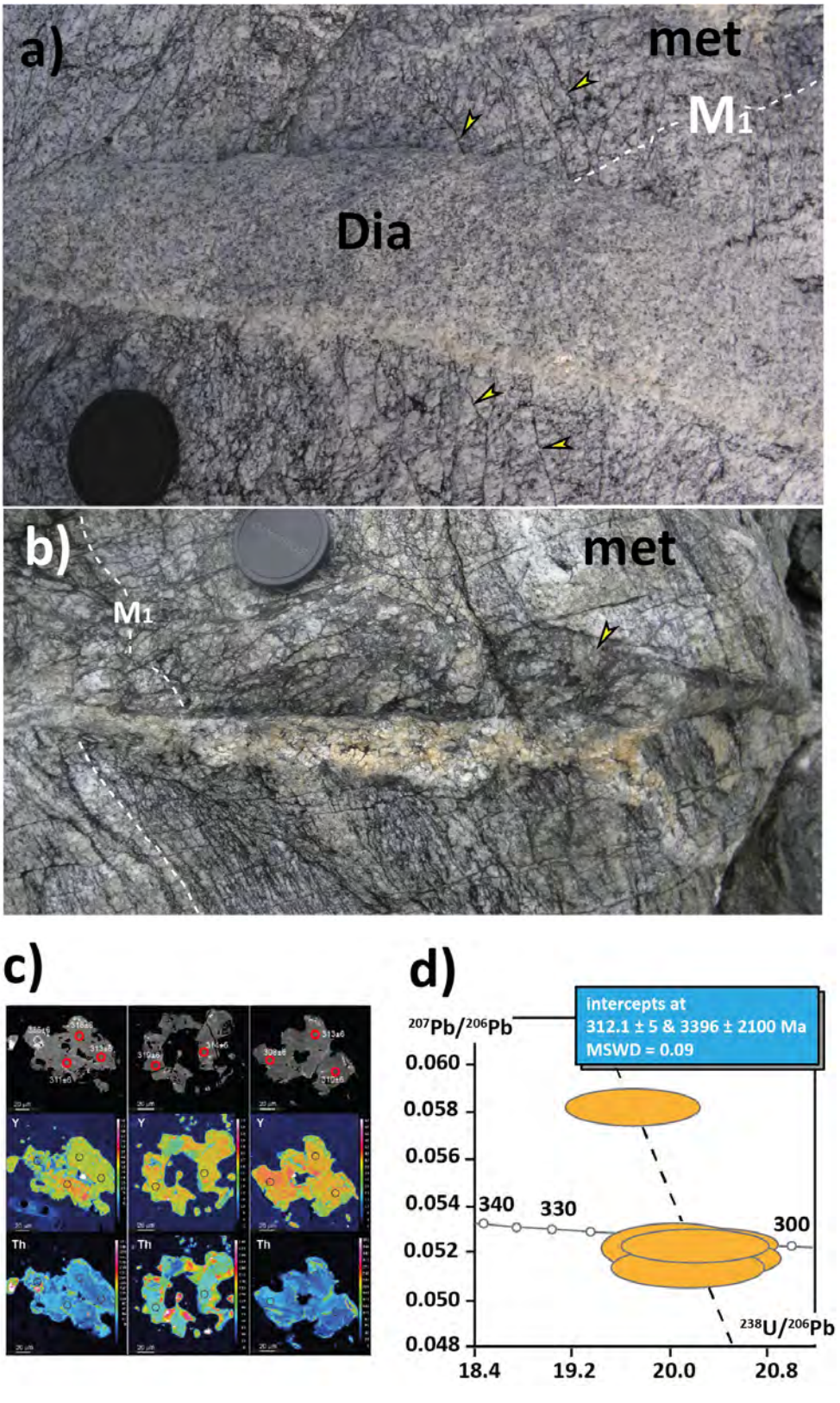

Fig. 21 - Co-seismic structures related to the M_2 melting stage: a) field relationships between pseudotachylytes-bearing faults (yellow stars), the diatexite (Dia) and the M_1 fabric of metatexite (met); b) close-up of a large pesudotachylyte-bearing fault (yellow stars) offsetting the M_1 fabric of metatexitic orthogneiss, here and in Fig. 21a about 10 cm-wide lens cap for scale; c) microstructural and micro-compositional features of monazite sampled within large pseudotachylyte veins, the red circles indicate the spot used to calculate the U-Pb age shown in Fig. 21d.

DAY 4

LATE VARISCAN MAGMATISM ACROSS THE CARBONIFEROUS-PERMIAN BOUNDARY

The fourth day of the field trip take place mostly in abandoned quarries close to the Arzachena village, focusing on late Variscan magmatism and particularly the transition from U_{2a} to U_{2b} magmatic stages in relation to the complex geodynamic setting resulting from plate reorganisation during post-orogenic shearing and bending of the orogen (i.e., Matte, 2001; Martinez-Catalan, 2011; Schulmann et al., 2009). U_{2a} granites (320 – 290 Ma; Casini et al., 2015a) such as the Arzachena Pluton, object of stops 4.1-4.3 are slightly peraluminous to metaluminous calc-alkaline rocks with distinctive mineralogical and geochemical fingerprints suggestive of a crustal source. The common assemblage is quartz + plagioclase + K-feldspar + biotite ± muscovite ± garnet. Amphibole is rarely present only within microgranular mafic enclaves and occasionally in the granodiorite groundmass. Zircon, apatite and sometimes monazite are present as accessory phases. Zircon grains very commonly preserve Ordovician to middle Proterozoic inherited cores, most ages being in the range Middle Ordovician–late Cambrian. The geochemical signature of the Arzachena Pluton is marked by negative εNd_{300} values <-6, high $^{87}Sr/^{86}Sr$ isotopic ratios >0.712, and low Mg# generally between 0.1-0.25 (Fig. 22a,c). The REE pattern is highly

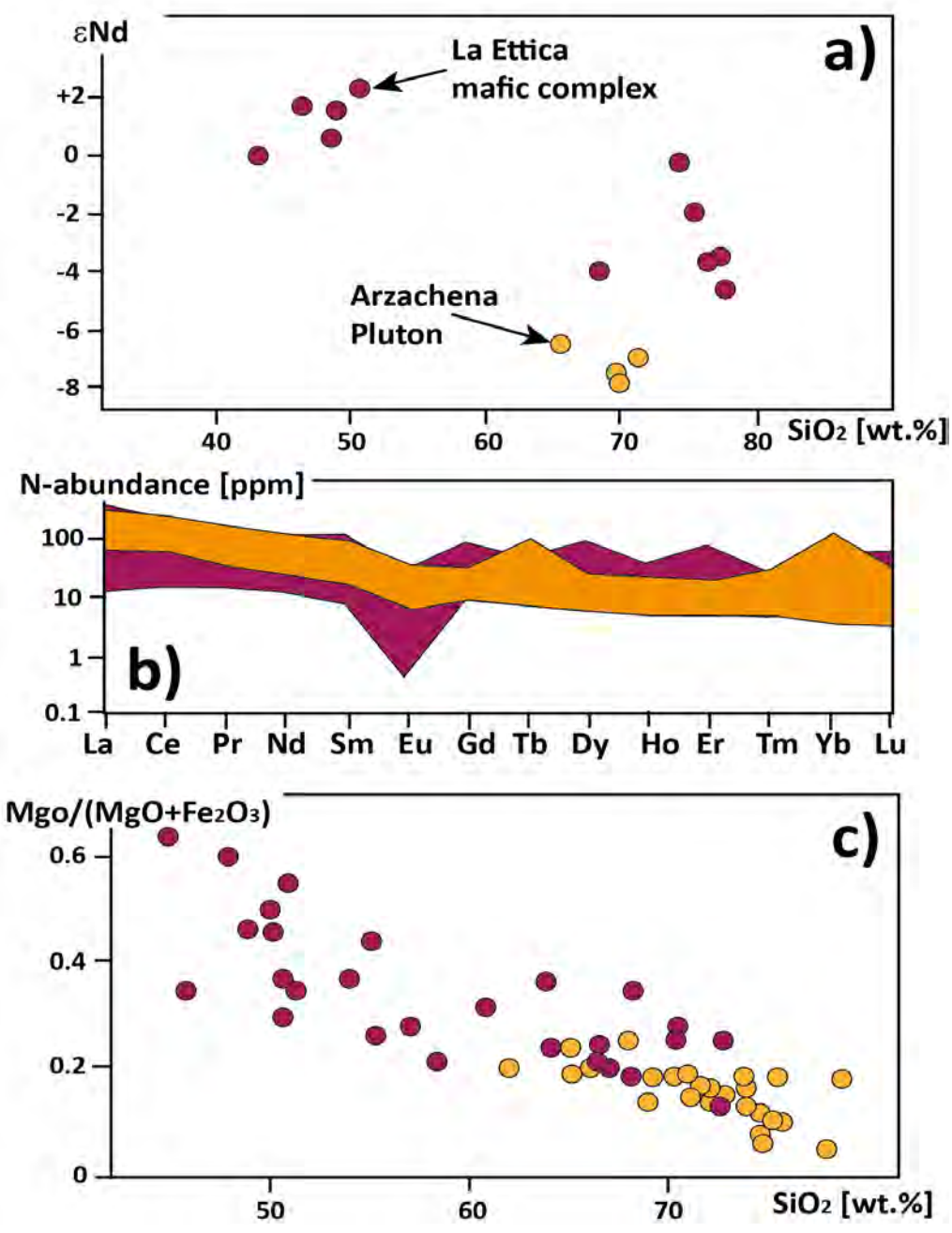

Fig. 22 - Main geochemical characteristics of the Arzachena pluton and La Ettica mafic complex: a) εNd values recalculated at the respective emplacement age of La Ettica mafic complex samples (magenta) and Arzachena pluton samples (orange); b) REE pattern; c) Mg# = $MgO/(MgO+Fe_2O_3)$.

fractionated defining a negative correlation between ΣREE and SiO_2 (Fig. 22b), with lower values (46.15 ppm) in leucogranites and maximum values of around 304.52 ppm in granodiorites (i.e., Casini et al., 2012, 2015a). The pluton is mostly anisotropic and characterised by an evident magmatic to HT sub-magmatic fabric consistent with horizontal flow of magma due to expansion of large, E-W oriented sill-shaped plutons (Fig. 23) emplaced in the upper crust (Casini et al., 2015a,b). U_{2b} rocks of the La Ettica mafic complex (285-288 Ma; Casini et al., 2015a,b) are compositionally much more heterogeneous, ranging from olivine-bearing gabbro to muscovite-bearing leuco-monzogranite. Basic to intermediate rocks are usually composed of amphibole + plagioclase ± pyroxene ± titanite ± apatite ± allanite, whereas felsic rocks are composed of quartz + plagioclase + K-feldspar + biotite ± muscovite ± apatite ± zircon. Amphibole is sometimes present in the groundmass. Unlike the trend observed in the Arzachena Pluton, the REE content of La Ettica complex rocks is positively correlated with SiO_2, the total REE content being 14.31 ppm in gabbroic rocks and 302.22 ppm in peraluminous monzogranite. All samples from the La Ettica complex have much more pronounced negative Eu anomalies (Fig. 22b) than in the Arzachena Pluton and fractionation is about half (i.e., Casini et al., 2012; 2015a). The εNd_{285} values show a great variability ranging from positive values between +2, +3 and <-4 (Fig. 22a).

In the field, several macroscopic differences can be observed between Arzachena and La Ettica outcrops. Micro-granular mafic enclaves (MME) are rare in the Arzachena Pluton and only rarely contain amphibole. On the other hand, metamorphic xenoliths are common. MME derived from mafic melts are relatively common within all facies of the La Ettica complex, including in the more felsic rocks (i.e., Casini et al., 2012, 2015a). Granites and basic rocks from La Ettica are characterised by a weak magmatic fabric and nearly no HT sub-solidus deformation, consistent with emplacement at very shallow crustal levels, likely <0.2 GPa (i.e., Casini et al., 2012). The mafic complexes and the magmatic fabric of the larger granitic plutons are normally oriented NE-SW, recording an abrupt change of the regional direction of maximum extension during the Carboniferous-Permian transition (Casini et al., 2015a,b). Clear field relationships (i.e., stops 4.4-4.5) coupled to thermobarometric estimates confirm the timing of magmatic stages indicated by U-Pb zircon dating and suggest that emplacement of the La Ettica gabbro occurred after substantial decompression and cooling of the Variscan crust, after a large clockwise rotation and displacement of the Corsica-Sardinia block along the south Variscan shear zone (i.e., Edel et al., 2014; Muttoni et al., 2003).

Stop 4.1 - The roof of Arzachena Pluton

Coordinates: Lat. 41°07'02"N, Long. 9°20'34"E
Location: Mte Mazzolu (Arzachena, SS)

A few km north-west of the Arzachena village (SS), the Lu Patenti Quarry on top of Mt. Mazzolu (266 m a.s.l.) exposes the apical zone of the Arzachena Pluton (320-308 Ma, Casini et al., 2012), which is one of the largest middle-Carboniferous granitic plutons of the Corsica-Sardinia Batholith (Casini et al., 2015a,b). Stop 4.1 can be reached from Arzachena village driving for about 5.6 km along the SS125 road in direction of Palau, up to a crossroads near a small country church dedicated to S. Giuseppe. Follow the road Surrau from the crossroads, then take the road Lu Patenti and continue up to the small dirt car park. The outcrop can be reached by a 10-minute walk on an easy footpath going uphill on the right of the car park area. On several polished cuts and well-exposed quarry levels, fresh 3D outcrops of the roof zone of the pluton can be observed (Fig. 23a). The area is characterised by strong compositional and textural layering marked by batches of garnet/epidote-bearing pegmatite and aplite, alternating with very fine-grained (grain size < 0.5 cm) leuco-monzogranite and more coarse-grained rocks such as slightly porphyritic monzogranite and granodiorite. The contacts between these different magmatic layers are gently dipping toward E-NE, roughly parallel to the contact between the pluton and the overlying metamorphic basement that is interpreted as the roof of the intrusion (Cuccuru et al., 2012).

Stop 4.2 - The wall-floor transition zone

Coordinates: Lat. 41°00'37"N, Long. 9°23'06"E
Location: S. Giacomo, SdF quarry (Arzachena, SS)

The second stop of day 4 can be accessed from the Arzachena village by car taking the SS427 road in direction of S. Antonio di Gallura. After about 9 km, turn to the left and follow the road to S. Giacomo locality. The outcrop is just on the left of the road, about 3.5 km from the crossroads with SS427 (Fig. 1c). Along the southern margin of the Arzachena Pluton close to S. Giacomo locality. From the car park area, a short and easy footpath takes to a small, abandoned quarry (SdF quarry) showing a fresh cut on the peripheral part of the pluton, made of relatively fine-grained, porphyritic biotite-bearing monzogranite. In the main level of the quarry, the granite shows a weak magmatic flow foliation, gently dipping toward the N-NE, or steeply dipping toward SSW, evidenced by the shape preferred orientation of cm-sized plagioclase crystals and K-feldspar phenocrysts, biotite schlieren and micro-

granitic/granodioritic enclaves. At places, batches of more differentiated fine-grained leuco-monzogranite showing ductile contact with the host porphyritic monzogranite can be observed (Fig. 23b). The zone characterised by steep S-dipping foliation is interpreted as the southern wall zone connecting the apical part of the pluton to its unexposed roots (i.e., Casini et al., 2012).

Stop 4.3 - The granodioritic core of the Arzachena Pluton

Coordinates: Lat. 41°04'35"N, Long. 9°20'54"E
Location: Punta Candela quarry (Arzachena, SS)

Stop 4.3 can be reached from the centre of Arzachena by driving along the road 'via G. Mameli' for about 2.3 km in

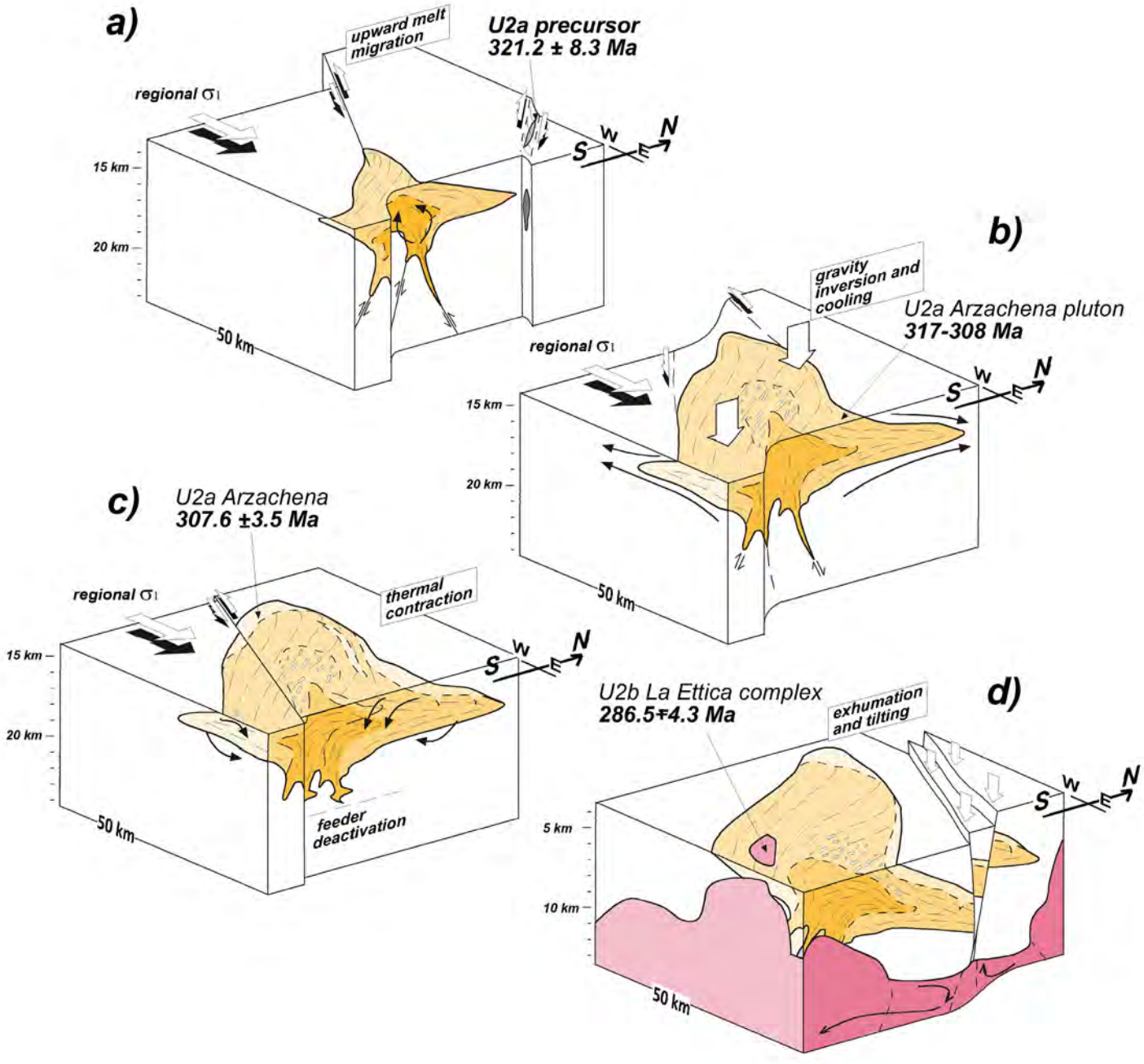

Fig. 23 - Structural model showing the relationships between the Arzachena pluton (U_{2a}) and the La Ettica mafic complex (U_{2b}): a) initial incremental growth of the Arzachena pluton through dyking, note that the pluton is mostly coeval with the oldest U_{2a} precursors emplaced within sub-vertical shear zones (i.e., Casini et al., 2012, 2015a, 2023); b) expansion stage of the Arzachena pluton with transition from vertical to lateral flow because of gravitational overturn due to inflation of magma; c) cooling stage of the Arzachena pluton yielding to thermal contraction and emplacement of differentiated high-SiO_2 melts into cooling fractures; d) emplacement of the La Ettica mafic complex after substantial exhumation of the Arzachena pluton during NE-directed extension of the Variscan crust (modified from Casini et al., 2012).

direction of Luogosanto - SP14 (Fig. 1c), up to a crossroads with a dirt road that goes toward west for about 880 m in direction of a huge outcrop just on top the rocky hill (Fig. 1c). Note that although most of the dirt road may be accessible by an offroad vehicle, it is recommended to park the car near the crossroads and continue by walking to not disturb the herds that are usually around. The outcrop exposes the deeper, relatively mafic, section of the Arzachena Pluton, dated here about 315-320 Ma by U-Pb ELA-ICP-MS on zircon (Casini et al., 2012). The rock is a medium-grained, porphyritic, biotite-bearing granodiorite with abundant fine-grained microgranular mafic enclaves, mostly composed of Ti-rich biotite, and hornblende (Fig. 23c). Small pegmatites and aplitic dikes of granodioritic composition can be observed at places. The shape preferred alignment of plagioclase crystals and mafic enclaves mark a strong magmatic flow foliation moderately to steeply dipping toward NNE-NE, which is interpreted as the shallower part of the root zone, consistently also with Al-in hornblende barometry supportive of emplacement pressure between about 0.35 to 0.40 GPa (Casini et al., 2012).

Stop 4.4 - The La Ettica Permian gabbro and quartz-diorite

Coordinates: Lat. 41°02'52"N, Long. 9°21'44"E
Location: Nuraghe la Prisjiona (Arzachena, SS)

Stop 4.4 can be reached from Arzachena village following the SS427 road toward S. Antonio di Gallura for about 4.4 km up to a crossroads, then follow the road 'Coddu Ecchju' for about 1.25 km up to the archaeological site 'Nuraghe la Prisjona' (Fig. 1c). The outcrop in the car park in front of the archaeological site exposes an early Permian sub-volcanic complex composed of fine-grained quartz-diorite, olivine-bearing gabbro, and fine-grained muscovite-bearing granodiorite emplaced at shallow crustal level (P<0.15 GPa, Casini et al., 2012). This small mafic complex, dated about 286 Ma (Cortesogno et al., 2007) intrudes the southern margin of the Arzachena Pluton forming a thick interaction zone, where the effect of mixing/mingling between felsic and mafic magmas and the effect of HT contact metamorphism can be observed. Within the archaeological site and also along the dirty road toward the final stop of the day, are exposed several small outcrops with abundant micro-granular mafic enclaves bearing hornblende ± pyroxene ± olivine assemblages and coarse-grained gabbro- to quartz-dioritic rocks grading to granodiorite.

Stop 4.5 - Magmatic breccias along the southern border zone

Coordinates: Lat. 41°01'54"N, Long. 9°21'13"E
Location: S. Paolo Calta church (Arzachena, SS)

The last stop of the day can be reached from the archaeological site by driving along the 'Coddu Ecchju' road for about 2.1 km up toward west up to the crossroads, then follow the 'via Paulu Calta' road up to the small country church and park along the road on the right some 500 m after the church site. Stop 4.5 can be reached from the car park walking through an easy 250 m-long footpath that goes northward uphill from the light pole in the car park area (Fig. 1c). The outcrop shows the contact between the Arzachena Pluton and the La Ettica mafic complex, which consists of magmatic breccias (Fig. 24d) highlighting the relationships and the relative timing between the mafic complex and the Carboniferous Arzachena Pluton. The contact zone exposes a variety of magmatic rocks ranging from relatively primitive compositions (gabbro, diorite) to more evolved ones (peraluminous granodiorite/monzogranite and fine-grained leuco-monzogranite), showing variable degree of mixing between both terms. A nice, polished outcrop of magmatic breccia composed of partly dismembered fragments of the Arzachena pluton embedeed within fine-grained leuco-monzogranite demonstrates that the more acidic terms of the La Ettica complex originated by contact melting of the Carboniferous Arzachena Pluton and the surrounding metapelitic metatexite.

https://doi.org/10.3301/GFT.2026.02

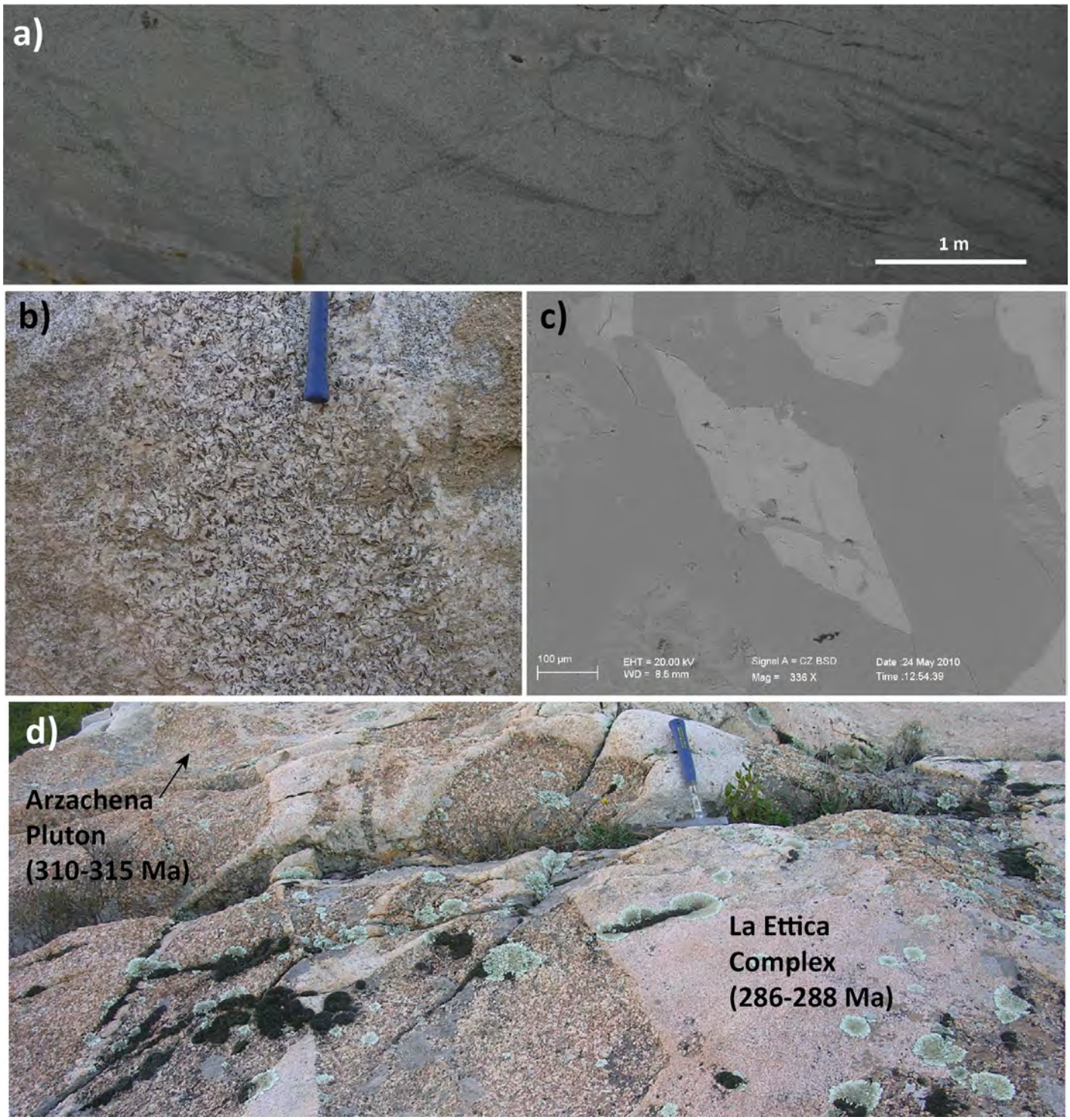

Fig. 24 - Field structural features of the Arzachena pluton: a) detail of the apical part of the pluton, note the magmatic layering marked by levels of fine-grained leucogranite, pegmatite and biotite schieren alternating to slightly coarser domains without any clear trend of grain size (the contact between the pluton and the metamorphic country rocks is a few tens of m upside, for reference); b) close-up of a biotite-rich pegmatitic domain in the leucogranite of the peripheral part of the pluton; c) SEM image of a idiomorphic hornblende crystal from the core of the Arzachena pluton, Pta Candela Quarry; d) magmatic breccias at the contact between the Arzachena Pluton and the La Ettica complex.

DAY 5

POST-VARISCAN EXTENSION AND MAFIC MAGMATISM– THE PUNTA FALCONE MAGMATIC COMPLEX

The Punta Falcone mafic complex (286 ± 4; Gaggero et al., 2007) is one of the best exposed early Permian intrusions (Fig. 25a) marking the end of Variscan magmatic activity in the Corsica-Sardinia Batholith (Casini et al., 2015a,b; Secchi et al., 2022). Despite its relatively small surface exposure (about 0.15 km^2), geophysical constraints indicate that most of the magmatic body likely continues offshore in the Bonifacio straits (Cassano et al., 1979). The more mafic terms of the complex are quite homogeneous being dominated by medium-grained gabbro to gabbronorite associated to subordinate leuco-gabbro, hornblende-bearing granodiorite and mafic pegmatites (Fig. 25b,c). Amphibole-bearing granites are also observed close to the western border of the mafic complex. Gabbroic rocks and host granitoids are in turn intruded within late Carboniferous granites of the S. Teresa pluton (307 +5/-2 Ma; Oggiano et al., 2005) and migmatites of the northern border of the Barrabisa shear zone (Casini et al., 2015a,b). Overall, the contacts between the mafic complex and the country rocks are sharp, as indicated by the occurrence of magmatic breccias, frequently deformed at HT and partly resorbed, and chilled margins composed of amphibole-bearing leuco-monzogranite grading to syenogranite (Fig. 25c).

In the field, all rock terms show frequently evidence of mixing and mingling between mafic and felsic endmembers (eastern contacts; Fig. 25c). Evidence of mafic/felsic interaction are also banded veins and schlieren observed in host pinkish granites, particularly along the western contact. Mafic rocks range in composition from gabbro/gabbronorite to quartz- monzogabbro/monzo-gabbronorite, whereas the felsic rocks show more varied compositions ranging from leuco-granodiorites to syenogranite on Q'-ANOR

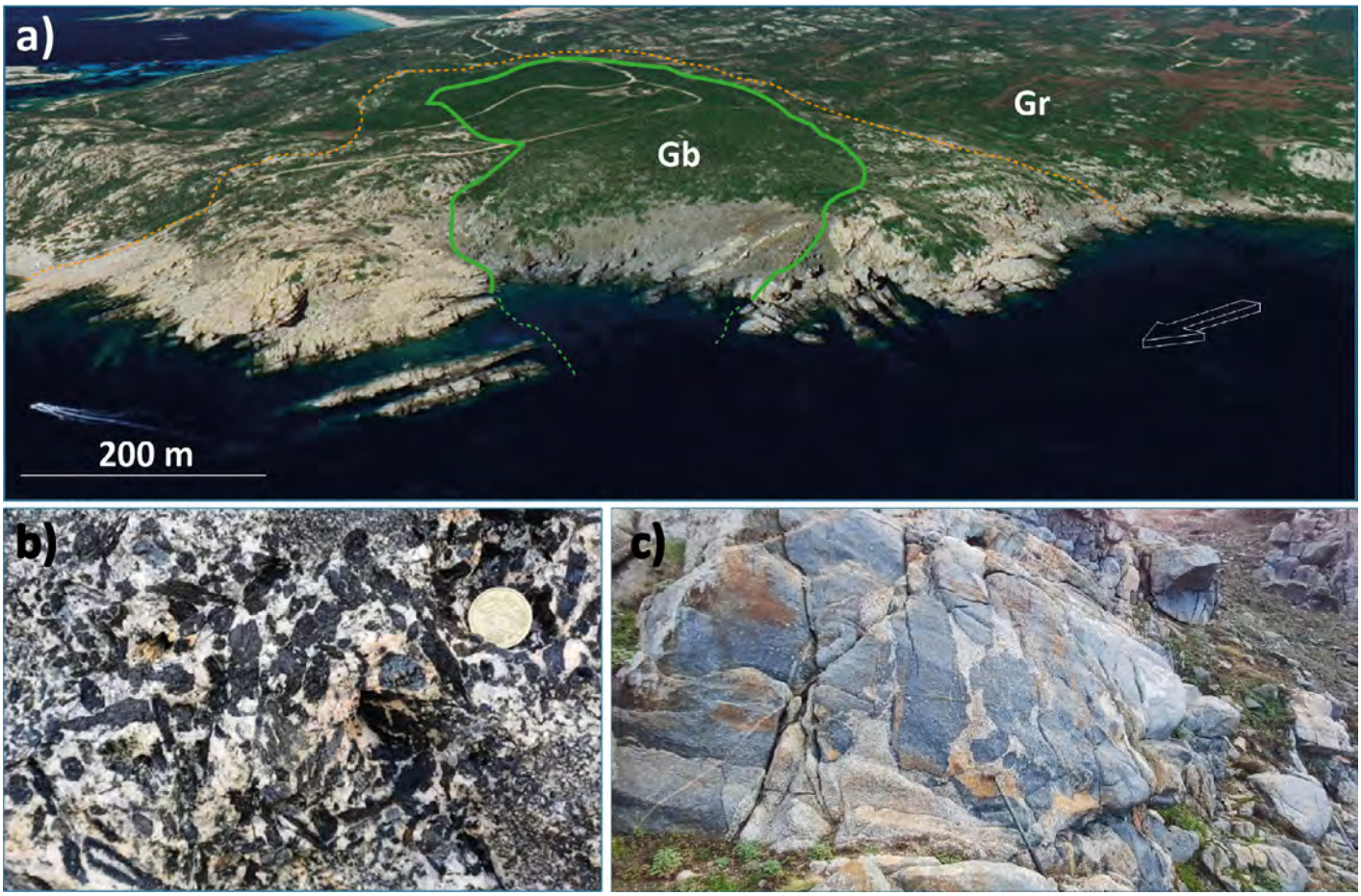

Fig. 25 - The Punta Falcone mafic complex: a) Google Earth view of the magmatic complex, Gb – undifferentiated mafic rocks (gabbro, gabbro-norite quartz-monzogabbro/monzogabbronorite), Gr undifferentiated felsic rocks (granite, granodiorite), the green and orange lines denote the boundary of the mafic complex and the border of the interaction zone between mafic rocks and their surroundings; b) hornblende pegmatites from gabbroic body at stop 5.2; c) evidence of mafic/acidic interaction along the eastern contact of Punta Falcone gabbroic body. Magmatic 'hot' breccias made of large fragments of gabbroic magma set within amphibole-bearing granodiorite. Note the occurrence of cm-sized feldspar xenocrysts in both relatively felsic and mafic terms.

diagram (Fig. 26a). Hornblende is also commonly observed in felsic rocks, particularly close to the contacts with the mafic complex. The samples show clearly a linear trend characterised by a marked gap between mafic rocks and the surrounding granites. Amphibole-only thermobarometry (Ridolfi, 2021) applied to calcic amphiboles both within mafic and felsic rocks indicates that gabbro and the coeval granites crystallised at low pressure between about 0.12-0.17 GPa (Fig. 26b), which is consistent with field observations and regional geology constraints (i.e., Gaggero et al., 2007; Casini et al., 2012, 2015a,b; Secchi et al., 2022). A pre-emplacement evolution at slightly higher pressure of about 0.4 GPa could be inferred for the mafic magma by clinopyroxene-only thermobarometry (Wang et al., 2021). In addition, evidence of interaction between mafic/acidic magma at upper crustal levels are offered by relatively high T estimates commonly >900°C for all rock types, and Log fO_2 at -14.5 (Fig. 26b). In summary, field and analytical data indicate that the Punta Falcone mafic intrusion represents an early Permian mantle-derived mafic complex which mixed at middle crustal levels (0.24-0.54 GPa) with a composite meta-igneous and metapelitic crust before final emplacement and cooling at sub-volcanic conditions, as already proposed for coeval early Permian plutonic complexes in south-eastern Sardinia (Secchi et al., 2022).

Stop 5.1 - Border of the Punta Falcone mafic complex

Coordinates: Lat. 41°15'26"N, Long. 9°13'32"E
Location: Punta Falcone (Santa Teresa di Gallura, SS)

The outcrops of the field trip (Stop 5.1, 5.2) can be reached from S. Teresa di Gallura village following the SS133bis road in direction of Palau for about 3.4 km. At the crossroads, follow the road for about 2 km and park in the eastern side of La Ficaccia village, just at the start of Punta Falcone road. Walk along the Punta Falcone dirt road for about 2 km up to a gate, then cross the gate on the left and continue along the Punta Falcone road for about 400 m up to a huge granitic cliff by the sea. Near the cliff, turn left downhill and make your way through the bushes to reach the small rocky cove (Fig. 1c). Here, stop 5.1 exposes the eastern border of the interaction zone between the Punta Falcone mafic complex and the surrounding granitic-metapelitic country rocks. The granitoids on the eastern and northern side of the rocky cove are extremely heterogeneous, at places layered, varying from fine-grained porphyritic leuco-monzogranite to coarse-grained granodiorite, sometimes amphibole-bearing. The compositional layering, at places strongly developed, is gently dipping toward N-NE, at high angle to the sub-vertical magmatic fabric preserved within the mafic body (see stop 5.2). Quartz and K-feldspar-bearing pegmatites are commonly observed within the granite, as well as partly assimilated magmatic breccias.

a)

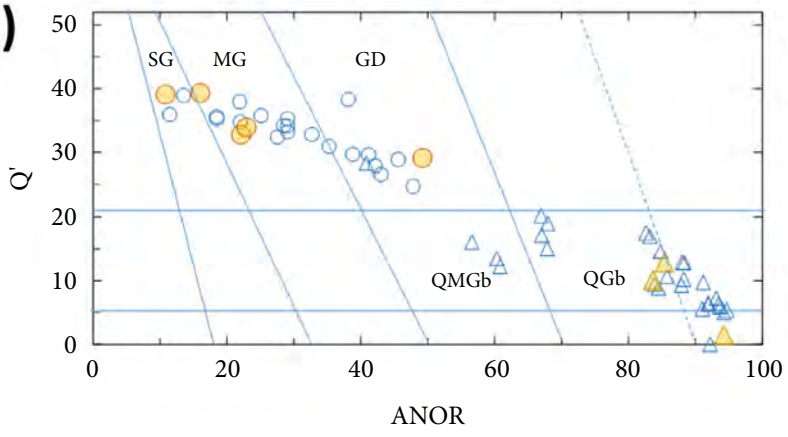

b)

	Gb		Gr
	Gb1	Gb2	Gr1
P_{Kbar}	**3.9** ± 1.5	1.5 ± 0.2	1.4 ± 0.2
T °C	**1094** ± 20	790 ± 22	785 ± 22
%H_2O	5.6 ± 1.5	7.0 ± 1.5	5.3 ± 0.9
LogfO_2	-11.4 ± 0.4	-14.5 ± 0.4	-14.5 ± 0.4

Fig. 26 - Geochemistry and thermobarometric estimates for the Punta Falcone mafic complex: a) Q'-ANOR classificative diagram for gabbroic (solid triangles) and host granitoids (solid squares) from Punta Falcone (northern Sardinia). %An_{Pl} of gabbroic rocks deduced by CIPW norm is in the range of 66 ÷ 73. Pale blue symbols refer to data after Poli and Tommasini (1991) and Tommasini and Poli (1992), reported for comparison. Q' = 100Q/(Q + Or + Ab + An). ANOR = 100An/(An + Or); fields according to Streckeisen and Le Maitre (1979). G, QGb, QMGb, GD, MG and SG refer to gabbro, Qz-gabbro, Qz monzo gabbro, granodiorite, monzogranite and syenogranite, respectively; b) PT conditions calculated according to Ridolfi (2021) on primary calcic amphiboles reported in Poli & Tommasini (1991) and Tommasini & Poli (1992) for gabbroic rocks (Gb1, Gb2) and surrounding granitoids (Gr1). Bold values denote T obtained from early crystallised clinopyroxene using the calibration of Wang et al. (2021) were interpreted as near liquidus conditions.

Stop 5.2 - Gabbro-diorite dykes of the feeder zone

Coordinates: Lat. 41°15'26"N, Long. 9°13'30"E
Location: Punta Falcone (Santa Teresa di Gallura, SS)

On the western side of the rocky cove (Fig. 1c), a superb outcrop exposes the eastern contact of Punta Falcone gabbroic body. The contact zone between the main gabbroic body and the surrounding granites is marked by a thick (100-200 m) interaction zone characterised by large (0.5-5m wide) fragments and blobs of gabbroic rock dispersed into pinkish heterogranular granite. These granites are usually porphyritic and highly heterogeneous varying from very fine-grained amphibole-bearing leuco-monzogranite to coarse-grained biotite and amphibole-bearing granodiorite. The porphyritic facies and granitic pegmatites are particularly frequent along the contact and can be observed in the small peninsula to the NE of the main mafic body.

ACKNOWLEDGEMENTS

This work has been developed within the framework of the project e.INS- Ecosystem of Innovation for Next Generation Sardinia (cod. ECS 00000038) funded by the Italian Ministry for Research and Education (MUR) under the National Recovery and Resilience Plan (NRRP) - MISSION 4 COMPONENT 2, "From research to business" INVESTMENT 1.5, "Creation and strengthening of Ecosystems of innovation" and construction of "Territorial R&D Leaders" granted to LC and AI. This research is partly funded by the University of Sassari (project DM737-SSCA granted to FAS). The authors greatly acknowledge the Asinara National Park for providing access to logistic facilities and for permission to sampling.

REFERENCES

Ballevre M., Bosse V., Ducassou C. & Pitra P. (2009) - Palaeozoic history of the Armorican Massif: Models for the tectonic evolution of the suture zones. C. R. Geosci., 341(2-3), 174-201.

Bonin, B. 2007 - A-type granites and related rocks: Evolution of a concept, problems and prospects. Lithos, 97, 1-29.

Bouchez J.L., Delas C., Gleizes G., Nédélec A. & Cuney M. (1992) - Submagmatic microfractures in granites. Geology, 20, 35-38.

Cappelli B., Carmignani L., Castorina F., Di Pisa A., Oggiano G. & Petrini R. (1992) - A Hercynian suture zone in Sardinia: Geological and geochemical evidence. Geodin. Acta, 5(1-2), 101-118.

Carmignani L., Carosi R., Di Pisa A., Gattiglio M., Musumeci G., Oggiano G. & Pertusati C. (1994) - The hercynian chain in Sardinia (Italy). Geodin. Acta, 7(1), 31-47.

Carosi R., Di Pisa A., Iacopini D., Montomoli C. & Oggiano G. (2004) - The structural evolution of the Asinara Island (NW Sardinia, Italy). Geodin. Acta, 17(5), 309-329

Carosi R., Frassi, C., Montomoli C. & Iacopini D. (2006) - Excursion in the Variscan basement of northern Sardinia (Italy): Field guide. J. Virtual Explor., 21, https://doi.org/10.3809/jvirtex.2006.00144.

Carosi R. & Oggiano G. (2002) - Transpressional deformation in northwestern Sardinia (Italy): Insights on the tectonic evolution of the Variscan Belt | Déformation transpressive dans le Nord-Ouest de la Sardaigne (Italie): Considérations sur l'évolution tectonique de la chaîne Varisque. C. R. Geosci., 334(4), 287-294

Carosi R. & Palmeri R. (2002) - Orogen-parallel tectonic transport in the Variscan belt of northeastern Sardinia (Italy): Implications for the exhumation of medium-pressure metamorphic rocks. Geol. Mag., 139, 497-511.

Carosi R., Montomoli C., Iacopini D., Petroccia A., Simonetti M. & Oggiano G. (2024) - Geology of the Asinara Island (Sardinia, Italy). J. Maps, 20(1), https://doi.org/10.1080/17445647.2024.2317136.

Carosi R., Montomoli C., Tiepolo M. & Frassi C. (2012) - Geochronological constraints on post-collisional shear zones in the Variscides of Sardinia (Italy). Terra Nova, 24, 42-51.

Casini L., Cuccuru S., Maino M., Oggiano G. & Tiepolo M. (2012) - Emplacement of the Arzachena Pluton (Corsica–Sardinia Batholith) and the geodynamics of incoming Pangea. Tectonophysics, 544-545, 31-49

Casini L., Cuccuru S., Puccini A., Oggiano G. & Rossi P. (2015a) - Evolution of the Corsica–Sardinia Batholith and late-orogenic shearing of the Variscides. Tectonophysics, 646, 65-78.

Casini L., Cuccuru S., Maino M., Oggiano G., Puccini A. & Rossi P. (2015b) - Structural map of Variscan northern Sardinia. J. Maps, 646, 65-78, https://doi.org/10.1080/17445647.2014.936914.

Casini L., Maino M., Langone A., Oggiano G., Corvò S., Reche J.-E. & Liesa M. (2023) - HT-LP metamorphism and fluid-fluxed melting during multi-stage anatexis of continental crust (N Sardinia, Italy). J. Metam. Geol., 41, 25-57, https://doi.org/10.1111/jmg.12687.

Casini L. & Funedda A. (2014) - Potential of pressure solution for strain localization in the Baccu Locci Shear Zone (Sardinia, Italy). J. Struct. Geol., 66, 188-204.

Casini L., Corvò S., Dulcetta L., Idini A., Langone A., Secchi F. & Maino M. (2025) - Convective mixing and geochemical differentiation of S-type plutons (Asinara Island, Italy). Lithos, 516-517, 108257.

Casini L. & Oggiano G. (2008) - Late orogenic collapse and thermal doming in the northern Gondwana margin incorporated in the Variscan Chain: a case study from the Ozieri Metamorphic Complex, northern Sardinia, Italy. Gondwana Res., 13, 396-406.

Cassano E., Marcello A., Nannini R., Pretti S., Ranieri G., Salvadori R. & Salvadori I. (1979) - Rilievo aeromagnetico della sardegna e del mare circostante. Servizio Geologico d'Italia 100, 7-30, Roma.

Cocco F., Loi A., Funedda A., Casini L., Ghienne J.-F., Pillola G.L., Vidal M., Meloni A.M. & Oggiano G. (2022) - Ordovician tectonics of the South European Variscan Realm: new insights from Sardinia. Int. J. Earth Sci., 112, 321-344.

Cocherie A., Rossi P., Fouillac A.M. & Vidal P. (1994) - Crust and mantle contributions to granite genesis - An example from the Variscan batholith of Corsica, France, studied by trace-element and NdSrO-isotope systematics. Chem. Geol., https://doi.org/10.1016/0009-2541(94)90186-4.

Conti P., Carmignani L. & Funedda A. (2001) - Change of nappe transport direction during the Variscan collisional evolution of central-southern Sardinia (Italy). Tectonophysics, 332, 255-273.

Conti P., Carmignani L., Oggiano G., Funedda A. & Eltrudis A. (1999) - From thickening to extension in the Variscan belt — kinematic evidence from Sardinia (Italy). Terra Nova, 11, 93-99.

Cortesogno L., Gaggero L., Oggiano G. & Paquette J.L. (2004) - Different tectono-thermal evolutionary paths in eclogitic rocks from the axial zone of the Variscan Chain in Sardinia (Italy) compared with the Ligurian Alps. Ofioliti, 29, 125-144.

Cortesogno L., Oggiano G., Buzzi L., Slejko F. & Gaggero L. (2007) - Post-variscan mafic dikes from the late orogenic collapse to the Tethyan rift : Evidence from Sardinia. Ofioliti, 32, 15-37.

Cruciani G., Franceschelli M., Jung S., Puxeddu M. & Utzeri D. (2008) - Amphibole-bearing migmatites from the Variscan Belt of NE Sardinia, Italy: Partial melting of mid-Ordovician igneous sources. Lithos, 105, 208-224.

Cruciani G., Dulcetta L., Franceschelli M., Beranoaguirre A., Millonig L.J. & Gerdes A. (2024) - In situ garnet U-Pb dating of granulitized eclogites from NE Sardinia. Italy. Ital. J. Geosci., 143(2), 226-236.

Cruciani G., Franceschelli M., Langone A. & Puxeddu M. (2019) - U-Pb zircon and Ar-Ar amphibole ages from Sardinian migmatites (Italy) and review of migmatite ages from the Variscan belt. Period. Mineral., 88, 2.

Cruciani G., Franceschelli M., Musumeci G., Spano M.E. & Tiepolo M. (2013) - U-Pb zircon dating and nature of metavolcanics and metarkoses from the Monte Grighini Unit: New insights on Late Ordovician magmatism in the Variscan belt in Sardinia, Italy. Int. J. Earth Sci., 102, 2077-2096.

Cruciani G., Franceschelli M., Puxeddu M. & Tiepolo M. (2018) - Metavolcanics from Capo Malfatano, SW Sardinia, Italy: New insight on the age and nature of Ordovician volcanism in the Variscan foreland zone. Geol. J., 53, 1573-1585.

Cruciani G., Franceschelli M., Caironi V. & Musumeci G. (2020) - U–Pb ages on detrital zircons and geochemistry of Lula paragneiss from Variscan belt, NE Sardinia, Italy: Implications for source rocks and early Paleozoic paleogeography. Ital. J. Geosci., 139(1), 131-148.

Cuccuru S., Gamboni A., Casini L. & Marini A. (2012) - I minerali di Monte Mazzolu. Cava 'Lu Patenti', Arzachena (OT) Sardegna. Riv. Mineral. Ital., 3, 168-181.

Cuccuru S., Naitza S., Secchi F., Puccini A., Casini L., Pavanetto P., Linnemann U., Hofmann M. & Oggiano G. (2016) - Structural and metallogenic map of late Variscan Arbus Pluton (SW Sardinia, Italy). J. Maps, 12(5), 860-865, https://doi.org/10.1080/17445647.2015.109175.

Cuccuru S., Casini L., Oggiano G. & Simula E.N. (2018) - Structure of the Castellaccio Pluton (Asinara Island, Italy). J. Maps, 14(2), 293-302.

Cuccuru S., Casini L., Oggiano G. & Cherchi G.P. (2012) - Can weathering improve the toughness of a fractured rock? A case study using the San Giacomo granite. Bull. Eng. Geol. Environ., 71, 557-567.

Debon F. & Le Fort P. (1988) - A cationic classification of common plutonic rocks and their magmatic associations: principles, method, applications. Bull. Minéral., 111(5), 493-510.

Denèle Y., Olivier P. & Gleizes G. (2008) - Progressive deformation of a zone of magma transfer in a transpressional regime: The Variscan Mérens shear zone (Pyrenees, France). J. Struct. Geol., 30, 1138-1149.

Del Moro A., Di Simplicio P., Ghezzo C., Guasparri G., Rita F. & Sabatini G. (1975) - Radiometric data and intrusive sequence in the Sardinian Batholith. Neues Jahrb. Mineral., Abh., 126, 28-44.

De Luca M., Ruberti N., Oggiano G., Rossi Ph., Pascucci V. & Casini L. (2023) - Structure of a Variscan migmatite-granite transition zone (N Sardinia, Italy). J. Maps, 19, 2182721, https://doi.org/10.1080/17445647.2023.2182721.

Di Vincenzo G., Carosi R. & Palmeri R. (2004) - The relationship between Tectono-metamorphic evolution and argon isotope records in white mica: constraints from in situ ^{40}Ar–^{39}Ar laser analysis of the Variscan basement of Sardinia. J. Petrol., 45(5), 1013-1043.

Di Pisa A., Oggiano G. & Talarico F. (1993) - Post collisional tectono-metamorphic evolution in the axial zone of the Hercynian belt in Sardinia: The example from the Asinara island. Doc. B.R.G.M., 219, 216-217

Edel J.B., Casini L., Oggiano G., Rossi P. & Schulmann K. (2014) - Early Permian 90° clockwise rotation of the Maures-Estérel-Corsica-Sardinia block confirmed by new palaeomagnetic data and followed by a Triassic 60° clockwise rotation. Geol. Soc. Spec. Publ., 405, 1-29.

Elter F.M., Musumeci G. & Pertusati P.C. (1990) - Late Hercynian shear zones in Sardinia. Tectonophysics, 176, 387-404.

Ferrara G., Ricci C.A. & Rita F. (1978) - Isotopic ages and tectono-metamorphic history of the metamorphic basement of North-Eastern Sardinia. Contrib. Mineral. Petrol., 68, 99-106.

Ferré E.C. & Leake B.E. (2001) - Geodynamic significance of early orogenic high-K crustal and mantle melts: example of the Corsica Batholith. Lithos, 59, 47-67.

Franceschelli M., Puxeddu M. & Cruciani G. (2005) - Variscan metamorphism in Sardinia, Italy: review and discussion. J. Virtual Explor., 19, https://doi.org/10.3809/jvirtex.2005.00121.

Franceschelli M., Memmi I. & Ricci C.A. (1982) - Ca distribution between almandine-rich garnet and plagioclase in pelitic and psammitic schists from the metamorphic basement of North-Eastern Sardinia. Contrib. Mineral. Petrol., 80, 285-295.

Frost B.R. & Frost C.D. (2008) - A Geochemical Classification for Feldspathic Igneous Rocks. J. Petrol., 49, 1955-1969.

Gaggero L., Oggiano G., Funedda A. & Buzzi L. (2012) - Rifting and arc-related early Paleozoic volcanism along the North Gondwana margin: geochemical and geological evidence from Sardinia (Italy). J. Geol., 120(3), 273-292, https://doi.org/10.1086/664776.

Gaggero L., Oggiano G., Buzzi L., Slejko F. & Cortesogno L. (2007) - Post-Variscan mafic dykes from the late orogenic collapse to the Tethyan rift: evidence from Sardinia. Ofioliti, 32, 15-37.

Gaggero L., Gretter N., Langone A. & Ronchi A. (2017) - U–Pb geochronology and geochemistry of late Palaeozoic volcanism in Sardinia (southern Variscides). Geosci. Front., 8, 1263-1284.

Ghezzo C. & Orsini J.B. (1982) - Lineamenti strutturali e composizionali del batolite Ercinico sardo-corso in Sardegna. In: Carmignani L., Cocozza T., Ghezzo C., Pertusati P.C., Ricci C.A. (Eds). Guida alla Geologia del Paleozoico Sardo pp. 165-181.

Giacomini F., Bomparola R.M. & Ghezzo C. (2005) - Petrology and geochronology of metabasites with eclogite facies relics from NE Sardinia: constraints for the Palaeozoic evolution of Southern Europe. Lithos, 82, 221-248.

Giacomini F., Bomparola R.M., Ghezzo C. & Guldbransen H. (2006) - The geodynamic evolution of the Southern European Variscides: constraints from the U/Pb geochronology and geochemistry of the lower Palaeozoic magmatic-sedimentary sequences of Sardinia (Italy). Contrib. Mineral. Petrol., 152, 19-42.

Giacomini F., Dallai L., Carminati E., Tiepolo M. & Ghezzo C. (2008) - Exhumation of a Variscan orogenic complex: insights into the composite granulitic–amphibolitic metamorphic basement of south-east Corsica (France). J. Metamorph. Geol., 26, 403-436.

Graziani R., Montomoli C., Iaccarino S., Menegon L., Nania L. & Carosi R. (2020) - Structural setting of a transpressive shear zone: insights from geological mapping, quartz petrofabric and kinematic vorticity analysis in NE Sardinia (Italy). Geol. Mag., 157, 1898-1916, https://doi.org/10.1017/S0016756820000138.

Green E.C.R., White R.W., Diener J.F.A., Powell R., Holland T.J.B. & Palin R.M. (2016) - Activity–composition relations for the calculation of partial melting equilibria in metabasic rocks. J. Metamorph. Geol., 34(9), 845-869, https://doi.org/10.1111/jmg.12211.

Gumiaux C., Gapais D., Brun J.P., Chantraine J. & Ruffet G. (2004) - Tectonic history of the Hercynian Armorican Shear belt (Brittany, France). Geodin. Acta, 17(4), 289-307, https://doi.org/10.3166/ga.17.289-307.

Gutiérrez-Alonso G., Fernández-Suárez J., Weil A.B., Murphy B.J., Nance D.R., Corf F. & Johnston S.T. (2008) - Self-subduction of the Pangaean global plate. Nat. Geosci., 1, 549-553.

Helbing H., Frisch W. & Bons P.D. (2006) - South Variscan terrane accretion: Sardinian constraints on the intra-Alpine Variscides. J. Struct. Geol., 28(7), 1277-1291.

Kruhl J. (1996) - Prism and basal-plane parallel subgrain boundaries in quartz: a microstructural geothermobarometer. J. Metamorph. Geol., 14, 581-589.

Idini A. Fancello D., Mameli P., Ferrero S., Cuccuru S. & Casini L. (2025) - A mineralogical perspective on the granite alkali feldspar megacrysts paradox. Lithos, https://doi.org/10.1016/j.lithos.2025.108229.

Laporte D., Fumey-Humbert F., Michon G., Orsini J.B. & Fernandez A. (1986) - The granitoids of Balagne (north-western Corsica): a complex of syntectonic Mg-K rich calc-alkaline intrusions. [Sur le caractere syntectonique des granitoides calcoalcalins magnesio-potassiques de Balagne (Corse du Nord-Ouest).] C. R. Acad. Sci., 303, 1321-1326.

Lister G.S. & Snoke A.W. (1984) - SC mylonites. J. Struct. Geol., 6(6), 617-638, https://doi.org/10.1016/0191-8141(84)90001-4.

Maino M., Casini L., Boschi C., Di Giulio A., Setti M. & Seno S. (2020) - Time-Dependent Heat Budget of a Thrust from Geological Records and Numerical Experiments. J. Geophys. Res. Solid Earth, 125(3), e2019JB018940. https://doi.org/10.1029/2019JB018940.

Martinez-Catalan J.R. (2011) - The Central Iberian arc, an orocline centered in the Iberian Massif and some implications for the Variscan belt. Int. J. Earth Sci., 101, 1-16.

Matte P. (2001) - The Variscan collage and orogeny (480–290 Ma) and the tectonic definition of the Armorica microplate: A review. Terra Nova, 13(2), 122-128.

Martínez Catalán J.R., Schulmann K. & Ghienne J.-F. (2021) - The Mid Variscan Allochthon: keys from correlation, partial retrodefor mation and plate-tectonic reconstruction to unlock the geometry of a non-cylindrical belt. Earth-Sci. Rev., 220, 103700, https://doi.org/10.1016/j.earscirev.2021.103700.

Muttoni G., Kent D.V., Garzanti E., Brack P., Abrahamsen N. & Gaetani M. (2003) - Early Permian Pangea 'B' to Late Permian Pangea 'A'. Earth Planet. Sci. Lett., 215, 379-394.

Oggiano G., Cherchi G.P., Aversano A., Di Pisa A., Ulzega A., Orrù P. & Pintus C. (2005) - Note Illustrative della Carta Geologica d'Italia alla scala 1:50.000, F. 428 Arzachena 144 pp., ISPRA, Roma.

Oggiano G. & Di Pisa A. (1988) - I graniti peralluminiferi sin-tettonici nell'area di Aggius – Trinità D'Agultu e loro rapporti con le metamorfiti di alto grado della Bassa Gallura. Boll. Soc. Geol. It., 107, 471-480.

Oggiano G., Gaggero L., Funedda A., Buzzi L. & Tiepolo M. (2010) - Multiple early Paleozoic volcanic events at the northern Gondwana margin: U-Pb age evidence from the Southern Variscan branch (Sardinia, Italy). Gondwana Res., 17(1), 44-58, https://doi.org/10.1016/j.gr.2009.06.001.

Padovano M., Dörr W., Elter F.M. & Gerdes A. (2014) - The East Variscan Shear Zone: Geochronological constraints from the Capo Ferro area (NE Sardinia, Italy). Lithos, 196-197, 27-41.

Palmeri R., Fanning M., Franceschelli M., Memmi I. & Ricci C.A. (2004) - SHRIMP dating of zircons in eclogite from the Variscan basement in north-eastern Sardinia (Italy). Neues Jahrb. Mineral., 6, 275-288.

Paquette J.-L., Ménot R.-P., Pin C. & Orsini J.-B. (2003) - Episodic short-lived granitic pulses in a post-collisional setting: evidence from precise U-Pb zircon dating through a crustal cross-section in Corsica. Chem. Geol., 198 1-20.

Paterson S.R., Fowler Jr. T.K., Schmidt K.L., Yoshinobu A.S., Yuan E.S. & Miller R.B. (1998) - Interpreting magmatic fabric patterns in plutons. Lithos, 44(1-2), 53-82, https://doi.org/10.1016/S0024-4937(98)00022-X.

Paterson S.R., Vernon R.H. & Tobisch O.T. (1989) - A review of criteria for the identification of magmatic and tectonic foliations in granitoids. J. Struct. Geol., 11, 349-363.

Pavanetto P., Funedda A., Northrup C.J., Scmitz M., Crowley J. & Loi A. (2012) - Structure and U-Pb zircon geochronology in the Variscan foreland of SW Sardinia, Italy. Geol. J., 47, 426-445.

Peng Z. & Redfern S.A. (2013) - Mechanical properties of quartz at the α-β phase transition: Implications for tectonic and seismic anomalies. Geochem. Geophys. Geosyst., 14(1), 18-28.

Pieruccioni D., Simonetti M., Iaccarino S., Montomoli C. & Carosi R. (2025) - Microstructural Investigation of Variscan Late-Collisional Granitoids (Asinara Island, NW Sardinia, Italy): New Insights on the Relationship Between Regional Deformation and Magma Emplacement. Geosciences, 15(3), https://doi.org/10.3390/geosciences15030108.

Poli G. & Tommasini S. (1991) - A geochemical approach to the evolution of granitic plutons: a case study, the acid intrusions of Punta Falcone (northern Sardinia, Italy). Chem. Geol., 92, 87-105.

Ridolfi F. (2021) - Amp-TB2: An Updated Model for Calcic Amphibole Thermobarometry. Minerals, 11, 324 https://doi.org/10.3390/min11030324.

Riel N., Kaus B.J.P., Green E.C.R. & Berlie N. (2022) - MAGEMin, an Efficient Gibbs Energy Minimizer: Application to Igneous Systems. Geochem. Geophys. Geosyst., 23(7), e2022GC010427.

Rossi P. & Cocherie A. (1991) - Genesis of a Variscan batholith. Field, petrological and mineralogical evidence from the Corsica-Sardinia batholith. In: Freeman R., Huch M., Mueller St. (Eds) The European Geotraverse part 7, Tectonophysics 195 319-346.

Rossi P., Oggiano G. & Cocherie A. (2009) - A restored section of the "southern Variscan realm" across the Corsica–Sardinia microcontinent. C. R. Geosci., 341(2-3), 224-238. https://doi.org/10.1016/j.crte.2008.12.005.

Schulmann K., Konopásekk J., Janoušek V., Lexa O., Lardeaux J.M., Edel J.B., Štípska P. & Ulrich S. (2009) - An Andean type Palaeozoic convergence in the Bohemian Massif. C. R. Geosci., 341 (2-3), 266-286.

Secchi F., Casini L., Cifelli F., Naitza S., Carta E. & Oggiano G. (2022) - Syntectonic magmatism and reactivation of collisional structures during late Variscan shearing (SW Sardinia, Italy). Int. J. Earth Sci., https://doi.org/10.1007/s00531-022-02193-2.

Siebel W., Blaha U., Chen F. & Rohrmüller J. (2004) - Geochronology and geochemistry of a dyke–host rock association and implications for the formation of the Bavarian Pfahl shear zone, Bohemian Massif. Int. J. Earth Sci., 94, 8-23.

Streckeisen A. & Le Maitre R.W. (1979) - A chemical approximation to the modal QAPF classification of the igneous rocks. N. Jahrb. Mineral. Abt., 136, 169-206.

Sylvester P.J. (1998) - Post-collisional strongly peraluminous granites. Lithos, 45, 29-44.

Tommasini S. & Poli G. (1992) - Petrology of the late-Carboniferous Punta Falcone gabbroic complex, Northern Sardinia, Italy. Contrib. Mineral. Petrol., 110, 16-32.

Vernon R.H., Johnson S.E. & Melis E.A. (2004) - Emplacement-related microstructures in the margin of a deformed pluton: the San José tonalite, Baja California, México. J. Struct. Geol., 26, 1867-1884.

Von Raumer J.F., Stampfli G.M. & Bussy F. (2003) - Gondwana-derived microcontinents — the constituents of the Variscan and Alpine collisional orogens. Tectonophysics, 365, 7-22.

Von Raumer J.F., Finger F., Veselá P. & Stampfli G.M. (2014) - Durbachites-Vaugnerites - a geodynamic marker in the central European Variscan orogen. Terra Nova, 26, 85-95.

Wang X., Hou T., Wang M., Zhang C., Zhang Z., Pan R., Marxer F. & Zhang H. (2021) - A new clinopyroxene thermobarometer for mafic to intermediate magmatic systems. Eur. J. Mineral., 33, 621-637.

Manuscript received 04 November 2025; accepted 23 January 2026; published online 26 February 2026;
editorial responsibility and handling by D. Pieruccioni.